Chiral Dynamics in Photo-Pion Physics: Theory, Experiment, and Future Studies at the HIγS Facility

Aron M. Bernstein
Department of Physics and Laboratory for Nuclear Science,
Massachusetts Institute of Technology,
Cambridge, MA 02139, USA

Mohammad W. Ahmed
Department of Physics and
Triangle Universities Nuclear Laboratory,
Duke University, Durham, NC, 27708-0308, USA

Sean Stave
Department of Physics and
Triangle Universities Nuclear Laboratory,
Duke University, Durham, NC, 27708-0308, USA

Ying K. Wu
Department of Physics and
Triangle Universities Nuclear Laboratory,
Duke University, Durham, NC, 27708-0308, USA

Henry R. Weller
Department of Physics and
Triangle Universities Nuclear Laboratory,
Duke University, Durham, NC, 27708-0308, USA

April 20, 2009

Abstract

A review of photo-pion experiments on the nucleon in the near threshold region is presented. Comparisons of the results are made with the predictions of the low energy theorems of QCD calculated using chiral perturbation theory (ChPT) which is based on the spontaneous breaking of chiral symmetry as well as its explicit breaking due to the finite quark masses. As a result of the vanishing of the threshold amplitudes

in the chiral limit, the experiments are difficult since the cross sections are small. Nevertheless the field has been brought to a mature stage of accuracy and sensitivity. The accomplishments and limitations of past experiments are discussed. Future planned experiments at Mainz and HIγS using polarization observables are discussed as a more rigorous test of theoretical calculations. Emphasis is given to the technical developments that are required for the HIγS facility. It is shown that future experiments will provide more accurate tests of ChPT and will be sensitive to isospin breaking dynamics due to the mass difference of the up and down quarks.

1 Introduction

The fundamental nature of threshold photo- and electro-pion production processes on the nucleon (N) has long been recognized [1] due to the fact that as a result of the spontaneously hidden (broken) chiral symmetry in QCD [2, 3, 4] the pion is a Nambu-Goldstone Boson [5]. Early work with the low energy theorems of current algebra made predictions for the s-wave amplitudes for the $N(\gamma,\pi)$ reaction [6, 7, 8, 9, 10]. Later, an effective-field-theory for QCD called chiral perturbation theory (ChPT) was employed [5, 11, 12, 13, 14, 15, 16, 17]. This is an expansion in momentum and pion (light quark) masses which are small compared to the chiral symmetry breaking scale of $\simeq$ 1 GeV. Since the perturbation series is truncated at a finite order the effect of the higher order neglected terms can be estimated to determine the theoretical error. The main point is that these calculations should be a close approximation to QCD, and that any discrepancy between ChPT theory and experiment which are larger then the estimated errors must be taken seriously.

ChPT with one-pion-loop corrections ("one-loop order") has been used to calculate the amplitudes for threshold photo- and electro-pion production from the nucleon [18, 19, 20, 21, 22, 23]. This theoretical development was driven by a series of threshold photoproduction experiments with high-duty-cycle accelerators carried out at Mainz [24, 25, 26] and Saskatoon [27]. Today there is impressive overall agreement between the ChPT calculations and the data. This agreement with a large body of data supports the concept of spontaneous chiral symmetry hiding in QCD [5, 11, 12, 13, 14, 15, 16, 17, 28].

The developments in photo-pion production followed similar work in the πN sector which is closely linked to photo-pion production by unitarity, or to put it more physically, by π-N interactions in the final states. As will be discussed, this leads to exciting opportunities to measure π-N phase shifts in properly designed photo-pion experiments. This requires transversely polarized targets to be fully exploited, and is one of the major issues which we expect to be experimentally studied for the first time in the next few years. Calculations of π-N interactions started with the current algebra predictions for pion-hadron scattering lengths [29]. Later calculations were performed with effective chiral Lagrangians [30] followed by a series of ChPT calculations [17, 31, 32] in low-energy πN scattering [17, 31, 32] which are in good agreement with experiment. Of particular importance is the precise measurement of π-N scattering lengths

in pionic hydrogen and deuterium [33]. These have been successfully interpreted with ChPT and require isospin breaking due to the Coulomb interaction [34, 35, 36].

The modern view is that QCD exhibits chiral symmetry when the light quark masses are set to zero (the chiral limit) in the Lagrangian. The absence of mass-degenerate parity doublets in the spectra of hadrons suggests that this symmetry is spontaneously broken (or hidden). The symmetry is not lost but appears in the form of massless, pseudoscalar, Nambu-Goldstone Bosons. Spontaneous symmetry breaking is well known in condensed matter physics, e.g. magnetic domains in iron which break the rotational symmetry of the Coulomb interaction. In this case, the Goldstone Bosons are spin waves or magnons. In QCD, the small non-zero light-quark masses explicitly break the chiral symmetry of the Lagrangian, with the result that the pion, eta and kaon have non-zero masses. Nevertheless, these eight pseudoscalar mesons are the lightest hadrons coming into the mass gap $\lesssim 1$ GeV.

As the lightest hadron, the pion best approximates the ideal Nambu-Goldstone Boson. In the chiral limit, where the light quark and pion masses $\to 0$, the pion would not interact with hadrons at low energies (i.e. the s-wave scattering lengths would vanish). In reality, the small mass makes the low energy interaction weaker than a typical strong interaction, but non-zero. The near-threshold interactions are important to measure since they are an explicit effect of chiral symmetry breaking and have been calculated by ChPT. In the future, lattice gauge theory is expected to also make accurate predictions. Since the occurrence of the quasi Nambu-Goldstone Bosons signifies spontaneous chiral symmetry breaking in QCD, their low-energy interactions with other hadrons, their electromagnetic production and decay amplitudes as well as their internal properties (e.g. radii, polarizabilities, decay) will serve as fundamental probes of the chiral structure of matter. These measurements represent timely issues since any disagreement between theory and experiment represents a possible failure of QCD. These measurements are often technical challenges for experimental physics.

The most precise tests of chiral dynamics are in the mesonic sector involving the Nambu-Goldstone Bosons(π, η,K)-particularly the pion, which is the lightest member of this family. In the past five years, there has been rapid progress in making such measurements. The recent NA48 high statistics experiment at CERN on the $K^{\pm} \to \pi^+\pi^- e^{\pm}\nu(K_{e4})$ and of the unitary cusp in the $K^{\pm} \to \pi^{\pm}\pi^0\pi^0$ decays is the process of accurately measuring the s-wave $\pi\pi$ scattering lengths [37]. These are found to be in agreement with ChPT calculations to two-loop order and with lattice calculations [38], and represent a critical test of chiral dynamics and of the basic assumption of symmetry which is spontaneously hidden and explicitly broken by the small, but finite, light quark masses. This agreement was achieved by also including the isospin breaking [38]

In addition, experiments on pionic hydrogen and deuterium at PSI have measured the s-wave πN scattering length [33] which was found to be in agreement with calculations provided that the Coulomb contribution to isospin breaking was taken into account [34, 35, 36]. On an equal chiral footing, the amplitude for

neutral pion photoproduction vanishes at low energies in the chiral limit. Existing data for this small magnitude [26, 27] are in reasonable agreement with ChPT calculations [18, 19, 20, 21]. Overall, these pion scattering and production experiments strongly support our underlying concept of the pion as a quasi Nambu-Goldstone Boson, reflecting spontaneous chiral symmetry breaking in QCD [28].

Despite these successes, not all of the chiral predictions have been properly tested. The long-standing prediction of Weinberg [30] that the mass difference of the up and down quarks leads to isospin breaking in πN scattering (in addition to the electromagnetic contribution) is of special interest in chiral dynamics. The accuracies of the completed experiments and of the model extractions from the deuterium pionic atom do not yet permit a rigorous test of this fundamental prediction. An interesting possibility is the use of the pion-photoproduction reaction with polarized targets to measure the isospin-breaking predictions of low energy $\pi^0 N$ scattering, which is related to the isospin-breaking quantity $\frac{m_d - m_u}{m_d + m_u} \simeq 30\%$ [30, 31, 32, 39]. This large value presents an unusual experimental opportunity since the general order of magnitude of the predicted isospin breaking is $\frac{m_d - m_u}{\Lambda_{QCD}} \simeq 2\%$. There have been claims of observing isospin breaking effects in medium-energy πN scattering experiments at several times this magnitude [40, 41]. These claims need independent testing! A proposed method to do this with photo-pion production [42] will be discussed in Sec. 5.2.

It is possible to characterize the successes of low energy πN and photo- and electro-pion production experiments as verifying that the pion is the approximate Nambu-Goldstone Boson of QCD, and that its low-energy production and interactions vanish in the chiral limit $m_u + m_d \to 0$ [28]. We can characterize the new generation of fully polarized photo-pion experiments that will be carried out at the HIγS facility and in Mainz as accurately testing the concept of spontaneous chiral symmetry breaking in QCD and the ChPT predictions based on this, and studying the consequences of $m_d - m_u > 0$.

2 Photopion Production Physics and πN Scattering

2.1 The Fermi-Watson (Final State Interaction) Theorem and Isospin Breaking Corrections

There is a deep connection between pion photoproduction and πN scattering. Formally, this occurs as a result of the unitarity of the S matrix. Physically, the connection is due to final-state interactions. In fact, since the photo-nucleon interaction is of small order ($e^2 \simeq \alpha$), the phase of the pion-photoproduction

multipole amplitudes is defined by the relationship:[1]

$$A^{2I}_{l,j} = e^{i\delta^{2I}_{l,j}} \widehat{A}^{2I}_{l,j} \tag{1}$$

where $\widehat{A}^{2I}_{l,j}$ are real functions of the CM energy, and can be identified as the multipole matrix elements for $\gamma p \to \pi N(I)$ in the absence of final state πN interactions. Equation 1 is the Fermi-Watson, or final state interaction, theorem when δ is identified as the elastic scattering πN phase shift [43, 44]. In comparison to the elastic πN scattering S matrix $= e^{2i\delta^{2I}_{l,j}}$, Eq. 1 shows that the phases of the πN multipoles enter with half the magnitude that they do in πN scattering. The Fermi-Watson theorem is very general, based on time-reversal invariance, three channel unitarity and isospin conservation. It is only valid below the two-pion threshold since the assumption of three channel unitarity is violated at higher energies. Strictly speaking it is not a true theorem since it must be modified if isospin conservation is not strictly valid.

When the Fermi-Watson theorem was derived, quarks were not known. It was assumed that isospin violation was caused only by electromagnetic effects of order $e^2 = \alpha$ and could be neglected. However, we now know there is an additional isospin-breaking mechanism due to the mass difference of the up and down quarks [31, 32, 30]. The modification of the Fermi-Watson theorem due to this mechanism has been worked out [28, 42, 45]. To generalize to the isospin breaking case, one can write the S-matrix for each quantum state $j = l \pm 1/2, I$ and total CM energy W as:

$$S^{2I}_{l,j}(\gamma p \to \pi N) = \begin{pmatrix} 1 & iA^1_{l,j} & iA^3_{l,j} \\ & \cos\psi\, e^{2i\delta^1_{l,j}} & i\sin\psi\, e^{i(\delta^1_{l,j}+\delta^3_{l,j})} \\ & & \cos\psi\, e^{2i\delta^3_{l,j}} \end{pmatrix} \tag{2}$$

where sin ψ represents an isospin-violating term and ψ is a real number which is a function W. For $\psi \to 0$, the isospin violation vanishes. The form of the 3x3 and 2x2 πN portions (lower right) of the S matrix have been chosen to be separately unitary and time-reversal invariant. Applying the unitary constraint $S^\dagger S = SS^\dagger = 1$, and assuming the weakness of the electromagnetic interaction by dropping terms of order e^2, one obtains [28, 42]:

$$\begin{aligned} A^1_{l,j}(\psi) &= e^{i\delta^1_{l,j}}[A^1_{l,j}(\psi=0)\cos\tfrac{\psi}{2} + iA^3_{l,j}(\psi=0)\sin\tfrac{\psi}{2}] \\ A^3_{l,j}(\psi) &= e^{i\delta^3_{l,j}}[A^3_{l,j}(\psi=0)\cos\tfrac{\psi}{2} + iA^1_{l,j}(\psi=0)\sin\tfrac{\psi}{2}] \end{aligned} \tag{3}$$

where $A^{2I(\psi)}_{l,j}(A^{2I}_{l,j}(\psi = 0))$ are the the $\gamma p \to \pi N$ multipoles with (without) isospin breaking interactions. As $\psi \to 0$, the isospin violation vanishes and the Fermi-Watson theorem is recovered. Strictly speaking the isospin label I for $A^{2I}_{l,j}(\psi)$ should not be included since it is not conserved. However, since the

[1]The notation is that A stands for the electric (E) or magnetic (M) multipole. The final state of the πN system in total angular momentum $j = l \pm 1/2$ (e.g, E_{0+} means electric dipole with $l = 0$ and $j = 1/2$), and isospin $I = 1/2$ or $3/2$. The total center-of-mass (CM) energy of the system W is implicit.

isospin violations are relatively small in magnitude, this approximate label is appropriate. As a consequence of Eq. 3, the phases of the πN multipoles should be measured, not calculated from the πN phase shifts (using the Fermi-Watson theorem), as they are now. To our knowledge, only one such measurement of the phases of the photoproduction multipoles has been performed [46], and that did not have the required precision to demonstrate a violation of the unmodified Fermi-Watson theorem.

2.2 Photopion Production in the Threshold Region and Isospin Violation

The effects of isospin breaking are dramatic in the threshold region. First, there is a significant charge-dependent energy difference between the thresholds for the $\gamma p \to \pi^0 p$ ($\pi^+ n$) reactions (144.7 and 151.4 MeV). For the region below the $\pi^+ n$ threshold, isospin is completely broken, since only one channel is open. However, even in this sub-threshold region, there is a strong influence of the charged-pion channel through the two-step $\gamma p \to \pi^+ n \to \pi^0 p$ reaction. Since the ratio of the electric dipole amplitudes for the neutral and charged pion channels $E_{0+}(\gamma p \to \pi^+ n)/E_{0+}(\gamma p \to \pi^0 p) \simeq -20$, the two step reaction is as strong as the direct path. This leads to a unitary cusp in the $\gamma p \to \pi^0 p$ reaction.

The simplest dynamical way to understand the occurrence of the unitary cusp in the $\gamma^* p \to \pi^0 p$ reaction (where γ^* is a real or virtual photon) is to use the 3-channel S matrix for the open channels $\gamma^* p, \pi^0 p$ and $\pi^+ n$ [42] (similar to Eq. 2). Applying the constraints of unitarity and time-reversal invariance, one is then led to the coupled-channel result for the s-wave amplitude $E_{0+}(\gamma p \to \pi^0 p)$:

$$\begin{aligned} E_{0+}(\gamma p \to \pi^0 p : k) &= e^{i\delta_0}[A(k) + i\beta q_+] \\ \text{with } \beta &= E_{0+}(\gamma p \to \pi^+ n) \cdot a_{cex}(\pi^+ n \to \pi^0 p) \end{aligned} \tag{4}$$

where δ_0 is the s-wave $\pi^0 p$ phase shift (predicted to be small), $A(k)$ is a smooth function of the photon energy k, β is the cusp parameter, $a_{cex}(\pi^+ n \to \pi^0 p)$ is the charge exchange s-wave scattering length for the $\pi^+ n \to \pi^0 p$ reaction and q_+ is the π^+ CM momentum[2] , which is continued below the $\pi^+ n$ threshold as $i \mid q_+ \mid$. The cusp function βq_+ contributes to the real (imaginary) part of E_{0+} below (above) the $\pi^+ n$ threshold. It is interesting that the constraints of unitarity show that the two-step $\gamma p \to \pi^+ n \to \pi^0 p$ mechanism is the most important energy dependence in the near-threshold $\gamma p \to \pi^0 p$ reaction. This is in agreement with the predictions of ChPT [18, 19, 20, 21].

The expected value of β can be calculated [42] on the basis of unitarity using Eq. 4. Note that the sign of β is observable, not just it's magnitude, and agrees with what is expected (see below). The best experimental value of $a(\pi^- p \to \pi^0 n) = -(0.122 \pm 0.002)/m_\pi$, obtained from the observed width in the 1s state of pionic hydrogen [33], was used. This is in excellent agreement with ChPT predictions of $-(0.130 \pm 0.006)/m_\pi$ [47]. Assuming isospin is conserved,

[2] With $a_{cex}(\pi^+ n \to \pi^0 p)$ in units of $1/m_{\pi^+}$ and q_+ in m_{π^+} units.

$a(\pi^+ n \leftrightarrow \pi^0 p) = -a(\pi^- p \leftrightarrow \pi^0 n)$. The latest measurement for $E_{0+}(\gamma p \rightarrow \pi^+ n) = 28.06 \pm 0.27 \pm 0.45$[3] [48] (where the first error is statistical and the second is systematic) is in good agreement with the ChPT prediction of 28.2±0.6 [49]. Using these experimental values and the relationship given above leads to a value of $\beta = 3.43 \pm 0.08$. On the other hand, the ChPT prediction (which does not satisfy unitarity) is $\beta = 2.78$ [18, 19, 20]. This difference is due to the truncation of the ChPT calculation at the one-loop $O(q^4)$ level. This value of β is at the π^+n threshold. For higher energies the value is proportional to the value of the $E_{0+}(\gamma p \rightarrow \pi^+ n; E_\gamma)$ amplitude (evaluated at photon energy E_γ) which is predicted to decrease with increasing E_γ [50].

The results for Re E_{0+} are presented in Fig. 1. The points are extracted from the latest data from Mainz [26]. The data on which they are based are not a complete experiment, which means that the multipoles cannot be extracted without some model assumptions. The errors shown in Fig. 1 are based on the experimental errors and do not include any model dependence. Future experiments which contain more polarization observables will reduce the model dependence of the analyses. Two curves are shown in Fig. 1. They are ChPT [21, 51] and a unitary fit [24]. On the basis of the data we have to date, they fit equally well. The anticipated improvements in the determination of this multipole based on 100 hours of beam time per observable at HIγS are also presented in the figure and will be discussed in detail in Sec. 5.2 (similar results could also be obtained at Mainz). Note that the sign of β has been measured to be positive as predicted; a negative sign would produce a predicted curve which is above the projected linear curves. In the future, the sign of β will be measured since the polarized target asymmetry $T(\theta) = A(y)$ is proportional to β. Thus the sign of this asymmetry is a direct measurement of the sign of β.

At the present time there are no measurements of Im $E_{0+}(\gamma p \rightarrow \pi^0 p)$. The predictions are presented in Fig. 1. The discrepancy in the values of β can be seen here. We anticipate that future experiments will provide a measurement at the 1-to-2% level and easily be able to distinguish between these predictions. From the results of the proposed measurement of Im E_{0+} one can extract $a_{cex}(\pi^+ n \rightarrow \pi^0 p)$ from the value of β using the experimental results for $E_{0+}(\gamma p \rightarrow \pi^+ n)$.

2.3 Isospin Violation at Intermediate Energies

As was discussed in Sec. 1, one expects isospin violations in πN scattering to be $\simeq \frac{m_d - m_u}{\Lambda_{QCD}} \simeq 4$ MeV/ 200 MeV = 2% [30]. However, it was shown that the electromagnetic effects reduce this to below 1% [31, 32]. Empirically, there have been two independent claims that isospin has been violated in medium-energy (30 to 70 MeV) πN scattering [40, 41]. Specifically, they showed that the "triangle relationship," which relates the amplitude of charge-exchange scattering

[3] The units for E_{0+} and β are $10^{-3}/m_\pi$, and for the scattering lengths are $1/m_\pi$.

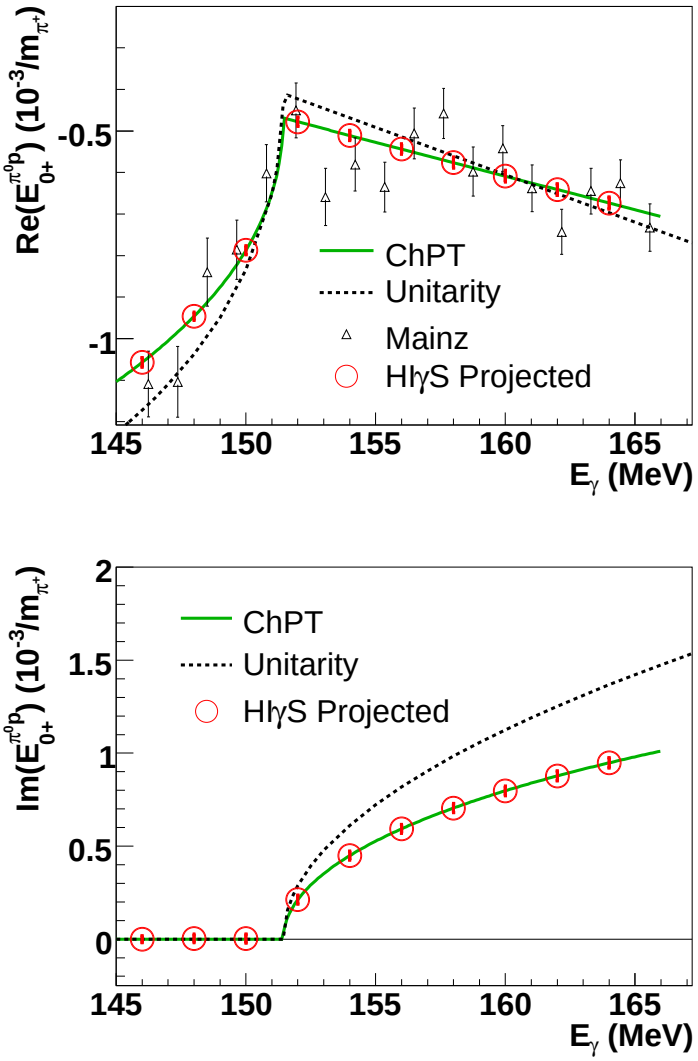

Figure 1: Upper panel: Re (E_{0+}) for the $\gamma p \to \pi^0 p$ reaction [26]. The solid curves are ChPT calculation [18, 19, 20, 21], and dashed curves are unitary fit [24, 25, 42] (see Eq. 4). Lower panel: Im (E_{0+}) for the $\gamma p \to \pi^0 p$ reaction [42]. For both panels the projected data points show the estimated statistical errors for 100 hours of beam time at HIγS at each energy in four different beam-target polarization configurations (see Fig. 7).

$(f(\pi^- p \to \pi^0 n))$ to the elastic scattering amplitudes $(f(\pi^{+(-)} p))$:

$$D \equiv f(\pi^- p \to \pi^0 n) - \frac{1}{\sqrt{2}}(f(\pi^+ p) - f(\pi^- p)) = 0 \tag{5}$$

does not hold. Instead they found

$$\begin{array}{c} D \simeq -0.012 \pm 0.003 \text{ fm} \\ D/f(\pi^- p \to \pi^0 n) \simeq 7\% \end{array} \tag{6}$$

about an order of magnitude larger than has been predicted by ChPT [31]. If true, this is a major discrepancy! However in a recent pion charge exchange experiment reported from TRIUMF [52] the results were consistent with a very small isospin breaking. The main difference between their conclusion and those of Gibbs and Matsinos [40] is due to an experimental discrepancy between two measurements of the pion charge exchange cross section. As will be shown below it is possible to measure the effect of isospin breaking using the transverse polarized asymmetry in photo-pion production. This is an entirely different reaction and does not depend on the measurement of cross sections!

The magnitude of the isospin-breaking effects in electromagnetic pion production can be obtained by assuming that they occur in the s-wave. Using Eq. 3 with $A^{2I}_{l,j}(\psi) = E^{2I}_{0+}(\psi)$, where I =1/2, 3/2 are two isospin states of the final πN system:

$$\delta E^{2I}_{0+} = E^{2I}_{0+}(\psi) - E^{2I}_{0+}(\psi = 0) \tag{7}$$

$$\text{which gives, for I=1/2, } \delta E^{1}_{0+} \simeq i\frac{\psi}{2} E^{3}_{0+}, \text{ and} \tag{8}$$

$$\text{for I=3/2 } \delta E^{3}_{0+} \simeq i\frac{\psi}{2} E^{1}_{0+} \ . \tag{9}$$

The approximation has been made that both the s-wave phase shifts and ψ are small, which is true in this energy region. This approximation, as well as assuming that the isospin breaking is in the s-wave, is easy to remove. It does serve to show that the two isospin states are indeed mixed, that the isospin mixing $\to 0$ as $\psi \to 0$ and that the multipoles pick up a small imaginary part due to this mixing. This implies that the time-reversal-odd observables (imaginary parts of bilinear products of the multipoles) will have to be measured to observe this effect. This will require polarized target experiments.

The empirical value of the isospin-breaking parameter ψ can be obtained from the measurements of D. From the 2x2 πN part of the S matrix, Eq. 2, one obtains [42]:

$$D = \frac{1}{2q} \sin\psi e^{(i\delta^1_{0,1/2} + i\delta^3_{0,1/2})} \ , \tag{10}$$

where it has been assumed that the isospin violation occurs in the s-wave, and $\delta^1_{0,1/2}(\delta^3_{0,1/2})$ are the s-wave πN phase shifts in the I=1/2 (3/2) state. Note that $D \to 0$ when $\psi \to 0$, as expected. The observed consequences of isospin breaking can be calculated for photoproduction using the empirical value of D.

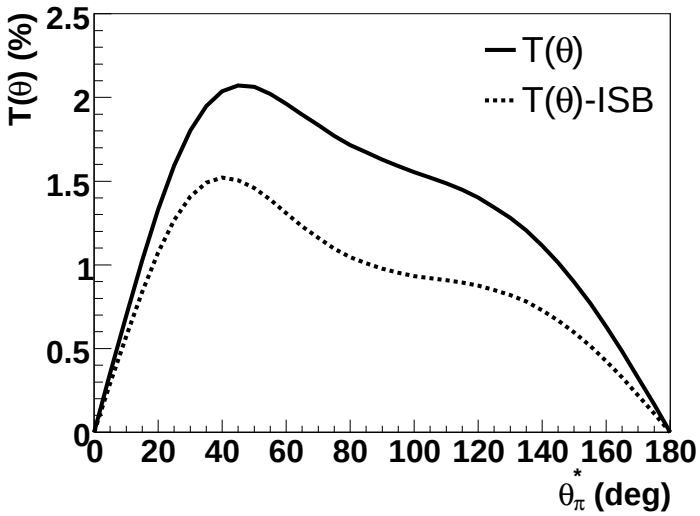

Figure 2: Polarized target asymmetry $\boldsymbol{A(y) = T(\theta)}$ in % for the $\gamma\vec{p} \to \pi^+ n$ reaction for W = 1120 MeV ($E_\gamma \simeq 200$ MeV). The target polarization is normal to the reaction plane. The solid curve is the prediction of the DMT model without isospin breaking ($T(\theta)$). The dotted curve is the DMT prediction if the empirical value of the isospin-breaking parameter $\psi = -0.010 \pm 0.004$ (Eq. 2) is used ($T(\theta) - ISB$)[42].

The simplest such observable is the polarized-target asymmetry. An example of this is given in Fig. 2. It can be seen that the relative effect is about twice as large in photoproduction as in pion scattering (15% versus 7%), making this a promising method to either confirm or dispute the reported isospin violation [40, 41]. It also should be pointed out that, in photoproduction, the final states ($\pi^0 p, \pi^+ n$) have little Coulomb interaction, which is one of the difficulties in analyzing pion-nucleon scattering data. The observation that the transverse polarized itarget asymmetry can be used to check isospin symmetry in the πN system is an example of the fact that this observable is sensitive to the πN phase shifts, and in fact can be used to measure them [53].

3 Experimental Facilities

Historically, experimental studies of Chiral Dynamics in photo-pion physics have been carried out at tagged photon facilities such as the Saskatchewan Accelerator Facility (SAL) [54] and the Mainz Microtron (MAMI) [55]. Future experiments, described in this review, are planned at the High Intensity γ-ray Source (HIγS). A brief review of the SAL and MAMI facilities and a somewhat more

detailed description of the less documented HIγS facility is presented here.

3.1 Mainz and tagged photon facilities

The SAL facility utilized a 300 MeV linear accelerator with a pulse stretcher ring (PSR) to produce a *c.w.* electron beam. The γ-rays were produced via bremsstrahlung in a narrow acceptance cone. The post-bremsstrahlung electrons were *tagged* by a focal plane detector. The γ-ray energy was defined by measuring the electron energy in a magnetic spectrometer and a time-of-flight coincidence between the tagged electron and the outgoing particles from the photo-induced reaction. The γ-ray beam was unpolarized and the tagger could be operated at a maximum rate of 1 MHz per channel [54].

At SAL, the (γ, π^0) measurements were carried out using the neutral pion spectrometer for low energy pion photoproduction Igloo [56], constructed from 68 lead glass Cherenkov counters. This calorimeter consisted of four faces to form a symmetric box. An energy resolution of $\sim$ 40 % was achieved at a photon detection energy of 100 MeV. The geometry was close packed which was good for the total cross section measurements, but suffered from poor angular resolution. An array of liquid scintillating detectors (BC-505) was used to detect the outgoing neutrons in the (γ, π^+) reaction. The SAL facility has since been shut down. A complete description of the SAL facility and experiments which were performed at SAL can be found in [57, 56, 27, 58, 59, 60, 48].

The MAMI facility uses coherent bremsstrahlung as a source of polarized γ-rays. Linear polarization of up to 80% can be achieved at γ-ray energies above pion threshold. The γ-rays at MAMI are tagged like those at the SAL facility. A tagging energy resolution of $\sim$ 1 to 2 MeV can be obtained in the γ-ray energy range of 40 - 800 MeV. The maximum tagging rate is $\sim$ 1 MHz per channel [61, 62].

Two different detector systems are available at MAMI for the detection of neutral pions. The first detector system, TAPS, consists of plastic BaF_2 scintillator telescopes. Accurate position information on the impact point of the γ-ray can be obtained as a result of the segmentation of crystals in TAPS ($\Delta \sim$ 30% of a single crystal diameter) [63]. This array was used for the measurement of the total cross section of the ^{1}H(γ, π^0) reaction as well as the photon asymmetry for π^0 production at 159.5 MeV γ-ray energy [26]. More recently, a 93 % of 4π NaI crystal array, Crystal Ball (CB), has been installed at MAMI. This detector consists of 672 NaI crystals, organized in two hemispheres. The geometric efficiency of CB is rather uniform in angle and energy as compared to TAPS and is subject to far smaller systematic errors, so that both the statistical and systematic errors will be vastly reduced. A new photo-pion experimental program is being planned using the crystal ball together with the TAPS detector as a forward wall, along with a central tracker. This combination of crystal ball and TAPS will provide a geometrical acceptance close to 4π combined with good energy and angular resolution for photopion experiments. The setup will also contain a frozen-spin polarized target which will enable the measurements of polarization observables on the nucleons.

3.2 HIγS Experimental Facility:Development and Upgrades

The High Intensity Gamma-ray Source (HIγS) at Duke University is a nearly monochromatic Compton γ-ray source with a very high flux, a wide energy range, and switchable polarizations. The current HIγS electron accelerators include a 0.18 GeV linear accelerator pre-injector, a 0.18 – 1.2 GeV booster injector, a 0.24 – 1.24 GeV storage ring, and several storage ring based Free-Electron Lasers (FELs). At HIγS, a high-intensity γ-ray beam is produced with a flux two to three orders of magnitude higher than other Compton gamma sources. The high flux performance is realized by colliding the electron beam in the storage ring with a temporally matched, high-power FEL beam built up inside a low-loss laser resonator. HIγS can be operated in a wide energy range from 1 MeV to about 100 MeV in the present configuration and with future upgrades above 100 MeV up to the pion threshold energy. This wide energy range is the result of selecting the lasing wavelength of the FEL and electron beam energy in the storage ring. Highly polarized gamma-ray beams can be produced with linear and circular polarizations using different FEL wiggler configurations. It is also possible to switch between the left- and right-helical polarizations on the minute or sub-minute time scale. Furthermore, as a dedicated Compton gamma source, HIγS can be optimized for specific research programs by operating in either the high-flux mode or high-resolution mode with a selectable temporal gamma-beam structure of a continuous wave (CW) or pulsed beam. Given these outstanding features, HIγS is a world-class Compton gamma-ray source for a wide range of scientific research programs in nuclear physics, astrophysics, medicine, and industrial applications.

While the first HIγS gamma beam was demonstrated in 1996 [64], the high performance of HIγS was only realized after a series of major upgrades of the associated accelerators and FELs in recent years. One of the major accelerator upgrades was the construction and commissioning of a 0.18 – 1.2 GeV compact synchrotron as a full-energy booster injector operating in a periodic injection mode (the "top-off" injection). Since its commissioning in 2006, this booster injector has enabled the high flux operation of HIγS in the higher energy region (above 20 MeV) in a so-called "electron-loss mode." In this mode, the booster periodically refills the storage ring in a top-off operation to maintain the electron beam current as Compton scattered electrons are lost at a substantial rate. In 2005, we also brought a new (OK-5) FEL into operation consisting of two helical wigglers which were installed in the same straight section as the older planar OK-4 wigglers. With this FEL upgrade, we gained the ability to produce gamma-ray beams with both linear and circular polarizations. The upgraded HIγS facility is shown in Fig. 3.

3.2.1 Capabilities of HIγS in the Present Configuration

The fully upgraded HIγS facility began user operation in 2007 with its performance exceeding the design specifications for the upgrades. The main operating parameters of HIγS accelerators and FELs are found in Ref. [65]. Since 2007,

the performance of HIγS has been improved further in two areas. Below 20 MeV in the so-called "no-loss mode" in which the Compton scattered electrons are retained in the storage ring, the gamma-beam flux has been increased by a factor of two to five using a very low loss (high-finesse) FEL cavity. The maximum total gamma-flux in this energy range exceeds 1×10^{10} γ/s. In the "electron-loss mode," by increasing the maximum magnetic field of the FEL wigglers, the projected maximum gamma beam energy of HIγS is increased to about 100 MeV using commercially available 190 nm FEL mirrors. The updated performance of HIγS gamma beams in the high flux mode is summarized in Table 1. The gamma-beam flux available for actual experimental use depends on collimation. For example, for a collimated gamma-ray beam with a 3 % full-width half-max energy spread, the on-target flux is about 4.5 % of the total flux given in Table 1.

3.2.2 HIγS Upgrades for 100 − 158 MeV Operation

With the current accelerator configuration of HIγS, the maximum gamma-beam energy is limited to about 100 MeV due to the availability of commercial FEL mirrors at the shortest wavelength of about 190 nm. The gamma-beam energy tuning range of HIγS for several FEL wavelengths are shown in Fig. 4. Due to a limited FEL gain and the need to build up the intracavity optical power for Compton scattering, the FEL operation requires highly reflective mirrors which are typically multi-layered dielectric mirrors. The mirror damage due to intense ultraviolet (UV) and vacuum-ultraviolet (VUV) radiation remains a serious problem in the wavelength regime below 190 nm.

A critical step to extend HIγS operation toward and beyond the pion-threshold energy is the development of highly reflective, radiation-resistive 150 nm FEL mirrors. This development will require advancing certain aspects of optical coating techniques in the vacuum ultra-violent (VUV) wavelength region. By closely collaborating with commercial optics companies, we project that useful 150 nm FEL mirrors will be available in the next few years and we will take advantage of any new advance with the VUV coating technology. As another important step toward operating the FEL at 150 nm, two additional OK-5 wigglers will be installed by the end of 2009 to form a four-wiggler FEL (see Fig. 3) in order to boost the FEL gain.

With 150 nm FEL mirrors, by operating the storage ring and booster up to maximum energy of 1.2 GeV, HIγS will be able to produce gamma-beams at energies up to around 158 MeV. Like operating in other energy region in the "electron-loss mode", the maximum gamma flux is expected to be limited by the electron beam injection rate. The projected initial performance is 1×10^8–2×10^8 γ/s total, and 5×10^8–1×10^9 γ/s after increasing the electron beam injection rate by upgrading the injectors.

3.2.3 A New Compton Gamma-source for High-flux Operation up to 220 MeV

Ground-breaking nuclear physics research requires a high energy gamma-ray

source with an on-target flux of 10^9 γ/s or higher. This level of flux performance is now within reach with a specially designed Compton gamma facility which takes advantage of the technological advances developed at HIγS and elsewhere. One of the key components is the availability of a very high power photon beam which has a temporal structure matched to that of the high-intensity electron beam. At HIγS, we have demonstrated the capability of producing a total gamma-flux of 10^{10} γ/s, or equivalently, an on-target flux on the order of 10^9 γ/s, for few MeV gamma beams in the "no-loss" mode, driven by an intense intracavity laser beam with a kW average power in the infrared or visible region. This level of high laser power is realized in a newly developed very low-loss FEL laser cavity with a finesse of $> 3 \times 10^3$. This development paves the way for achieving 10^9 γ/s gamma flux performance above 100 MeV with a few-GeV electron accelerator.

One of the possibilities for such a high-energy, high-flux Compton gamma source would consist of a 2.5 GeV storage ring and a 480 nm, kW FEL beam. Such a facility could produce gamma ray beams up to 220 MeV. The flux performance would mainly be limited by how fast the lost electrons can be replaced. For example, to produce a gamma beam with a flux of 10^9 γ/s and with a 3% full-width, half-max energy spread, a full-energy, top-off injector should be developed to refill the storage ring at a rate of about 3 nC per second. This is realizable with a booster injector running at a few Hz. An even higher flux is possible if the injector and storage ring are further optimized. This particular configuration is rather feasible because it utilizes the demonstrated accelerator and FEL technologies without pushing new technological limits.

An alternative method for producing a high-intensity laser beam is to use a very low loss (high-finesse) optical resonator driven by an external laser. This technology is still under development but may become mature enough to replace the FEL as the photon source for this future Compton gamma source.

Table 1: Parameters of HIγS gamma-ray beam in the high-flux mode (2008).

Parameter	Value	Comments
E-beam configuration	Symmetric two-bunch	
E-beam current [mA]	50 - 120	Total current
γ-ray energy, E_γ [MeV]		
With mirrors 1064 to 190 nm	1 – 100	With existing hardware
Total flux [γ/s]		
(a) No-loss mode ($\leq$ 20 MeV)		Both linear and circular
E_γ = 1 – 2 MeV	1×10^8 – $1 \times 10^{9\,(a)}$	polarization
E_γ = 2 – 20 MeV	1×10^9 – 1×10^{10}	
(b) Loss mode ($>$ 20 MeV)		Preferred Polarization
E_γ = 21 – 100 MeV	1×10^8 – $2 \times 10^{8\,(b)}$	Circular
Linear and Circular polarization	$> 95\%$	Depending on collimator size

$^{(a)}$ High flux horizontally polarized gamma-ray beams can be produced by the OK-4 FEL. The circularly polarized gamma-ray flux is lower due to the dynamic impact of the OK-5 wigglers.

$^{(b)}$ The flux is currently limited by the capability of sustaining a high intracavity power by the FEL mirrors and the electron injection rate.

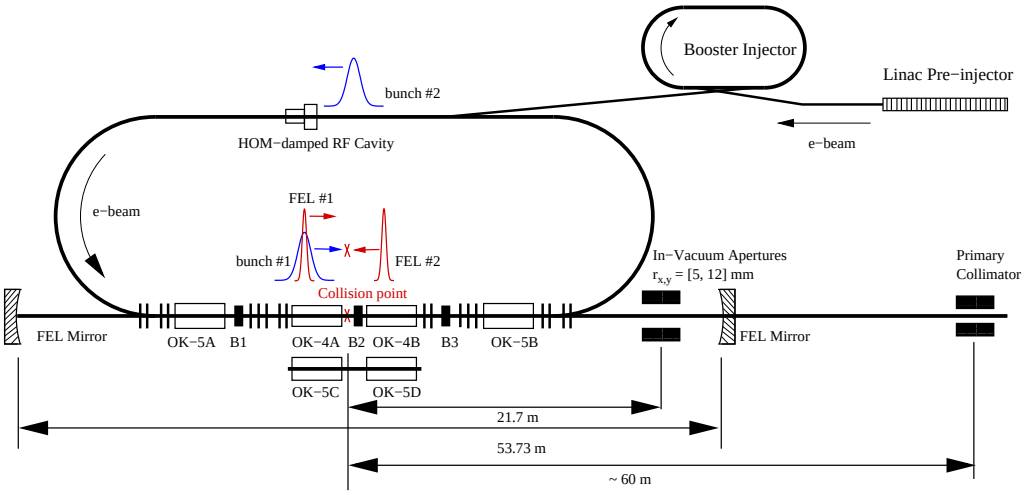

Figure 3: The schematic of HIγS facility in 2008 with two electron beam bunches colliding with the FEL pulses inside the FEL resonator cavity. The completed upgrade projects since 2004 include a new 0.18 to 1.2 GeV top-off booster synchrotron, a new 34 meter long storage ring straight section for hosting a higher order mode damped RF cavity and for a new injection scheme with the booster, and a new OK-5 FEL in the FEL straight section.

3.3 Experimental Setup at HIγS

The experimental setup for the proposed experiments at HIγS includes the following key resources : 1) Crystal Box detector [66]; 2) Neutral Meson Spectrometer (NMS) [67]; 3) Liquid Scintillating Neutron Detectors; and 4) HIγS Frozen-Spin Polarized Target (HIFROST). The Crystal Box detector consists of 270 NaI crystals arranged in three arrays of 9 $\times$ 10 crystals each. The size of each crystal is 2.5 in. $\times$ 2.5 in across and 12 radiation lengths long. The energy resolution ΔE/E (FWHM) of each array is $\sim$ 1.3 % at 100 MeV of photon detection energy. The NMS consists of 120 CsI crystals arranged in 2 arrays of 6 $\times$ 10 crystals each and $\sim$ 16 radiation lengths long. A detailed description of the Crystal Box and the NMS detectors can be found in [66, 67]. In addition, a variety of Liquid Scintillating Neutron Detectors are available at TUNL/HIγS for the detection of neutrons from the proposed ^{1}H(γ, π^+)n reaction. The most prominent of these detectors is the Blowfish array, which is a reconfigured version of the detectors used at SAL for the cross section measurement of the ^{1}H(γ, π^+)n reaction. Therefore, it is ideally suited for a similar measurement at HIγS with only minor modifications. A detailed description of the Blowfish array is available in [68] and references therein.

A frozen-spin polarized target (HIFROST) is being installed at HIγS. The HIγS target has a length of 7.3 cm, a diameter of 2.0 cm, and a target thickness

of $\sim 3.5 \times 10^{23}$ polarized protons per cm^2. The polarization is expected to be 70-80 %. The target is first polarized using a strong (4 T) field in a superconducting magnet and the polarization is maintained using superconducting *holding* coils at a lower ($\sim$ 0.24 T) field. These holding coils can be cylindrical to produce longitudinal polarization along the axis of the cylindrical target, or a pair of isolated *saddle*-shaped coils to provide polarization transverse to the axis of the cylindrical target. The longitudinal coils are a proven technology and have been used at Paul Sherrer Institute (PSI), MAMI, and JLab [69, 70]. The *saddle* coils are being developed in collaboration between TUNL and JLab. Recently, multiple *saddle* coils were prepared at JLab and tested for their maximum field strength. A Similar setup at TUNL is now ready to produce and test these saddle coils. Recent results indicate that the current design and production scheme of the saddle coils produces the desired field for the transverse polarized target. In addition, the collaboration is developing a *scintillating* frozen spin polarized target. The U.Va.–TUNL group in collaboration with the University of Massachusetts group (led by Rory Miskimen) and James Madison University (led by S. Whisnant), is planning to build such a scintillating-frozen-spin target. This target will be based on the experience of the group at the PSI which has constructed a polarized scintillating frozen-spin target [71]. We expect the non-scintillating HIFROST to be fully installed at HIγS by the summer of 2009, and the scintillating version available by mid-2010.

The π^0 from the ^{1}H(γ, π^0) reaction will be detected primarily by the Crystal Box with possible additional coverage by the NMS. One possible setup is placement of the three crystal box arrays in a triangular configuration, with their long edges touching one another and parallel to the beam direction. In this setup, the target is placed in the center of the triangle with the shortest distance from the target to each crystal box array being 6.5 in. At E$_\gamma$ of 158 MeV, this setup provides $\sim 3\pi$ solid angle coverage for π^0 detection. This could be enhanced to over $\sim$ 90% of 4π with the inclusion of the NMS in the setup. The energy of the neutral pion is inferred from its decay photons.

We expect a flux of $\sim 1 \times 10^8$ γ/s on target with an energy spread of $\sim$ 5 %. Since the γ-rays are produced using two electron bunches, they are produced in a pulsed mode with a repetition rate of 5.58 MHz (a beam burst every $\sim$ 179 ns). This pulsed structure of the beam helps in making the $time - of - flight$ technique a valuable resource in reducing non-beam related background. The γ-ray flux will be measured using a large NaI detector of known efficiency. This detector is placed directly in the beam with the flux reduced by inserting precision attenuators in the beam. Knowing the attenuation coefficients and the number of attenuators, a measurement of the total unattenuated flux can be obtained and used to calibrate a thin scintillating paddle. Monitoring the flux with this thin-scintillator provides a real-time flux determination. This attenuator system exists at HIγS and has been employed and tested to provide flux measurements to an accuracy of 3 to 7 %.

Details of the expected count rates and extraction of multipole moments to construct the desired observables is given in Sect. 5.

4 Photoproduction Observables with Full Polarization

4.1 Observables

The differential cross section for pion photoproduction in the center of mass system has the form [72]:

$$\begin{aligned} d\sigma/d\Omega_\pi &= (p_\pi^*/k_\gamma^*)\left\{R_T^{00} + \Pi_T {}^cR_{TT}^{00}\cos 2\varphi + P_x\left(-\Pi_T {}^s\boldsymbol{R_{TT}^{0x}}\sin 2\varphi + \Pi_\odot R_{TT'}^{0x}\right)\right. \\ &\left. + P_y\left(\boldsymbol{R_T^{0y}} + \Pi_T {}^c\boldsymbol{R_{TT}^{0y}}\cos 2\varphi\right) + P_z\left(-\Pi_T {}^s\boldsymbol{R_{TT}^{0z}}\sin 2\varphi + \Pi_\odot R_{TT'}^{0z}\right)\right\} \end{aligned} \quad (11)$$

where each R is a response function (bold-face response functions indicate a time reversal odd function), p_π^* and k_γ^* are the center of mass momenta of the pion and photon, respectively, φ is the angle between the photon polarization vector and the reaction plane, Π_T and $\Pi_\odot$ are the magnitudes of the photon's linear and circular polarization, respectively, on a scale from zero to one. The $P_{x,y,z}$ terms are the magnitudes of the target polarization in the πN center of mass reaction plane where z is the photon direction, x is transverse in the reaction plane, and y is transverse and perpendicular to the reaction plane. R_T^{00} is the unpolarized observable and ${}^cR_{TT}^{00}$ and R_T^{0y} are the single polarization observables. The notation denotes each response function for three different polarized target directions: R^{0x}, R^{0y},and R^{0z}. The four boldface symbols represent time reversal odd observables (TRO; imaginary parts of the bilinear products of the multipoles). The other four response functions are time reversal even (TRE; real parts of the bilinear products of the multipoles). The TRO amplitudes are crucial in measuring the phases of the amplitudes, which makes them more sensitive to the πN physics. The different terms in Eq. 11 can be separated by their dependence on φ, the target polarization directions, and by varying the sign of the linear and circular beam polarizations.

Equation 11 is in the CM system so we must Lorentz transform the observables from the laboratory system: this is taken as a right handed coordinate system in which the photon direction is $z_L = z$, x_L is transverse in the plane of the floor, and y_L is transverse and perpendicular to the plane of the floor. In this lab system we define the pion direction as θ_π^L, ϕ_π, so that the orientation of the reaction plane is ϕ_π (the value of ϕ is the same in the lab and the CM system). When the photon polarization is chosen parallel to $x_L(y_L), \varphi = \phi_\pi(\pi/2 - \phi_\pi)$. The value of θ_π in the CM system is obtained from $\tan(\theta_\pi) = \beta_\pi \sin(\theta_\pi)/[\gamma_{CM}(\beta_\pi \cos(\theta_\pi) - \beta_{CM})]$ where $\beta_\pi = p_\pi/E_\pi, \beta_{CM} = k/(k + M_p), \gamma_{CM} = (1 - \beta_{CM}^2)^{-1/2}$ and k is the photon energy in the lab system. We know the target polarization in the lab system where it has magnitude p_T, points in the direction θ_T, ϕ_T and its four vector is (1, $\vec{P_T}$). To obtain the target polarization in the CM system we have to perform another Lorentz transformation. As a consequence, the z component is transformed. The transverse target polarization components remain the same in magnitude as in the lab system $P_{xL} = P_T \sin(\theta_T)\cos(\phi_T), P_{yL} = P_T \sin(\theta_T)\sin(\phi_T)$. However care

must be taken in calculating P_x, P_y since these coordinates are defined relative to the pion production plane which is at angle ϕ_π relative to the lab plane. In this frame the y axis (normal to the reaction plane) is in the direction of $\hat{p_\pi^*} \times \hat{k}$ and $\hat{x} = \hat{y} \times \hat{k}$ where p_π^* is the pion center-of-mass (CM) momentum. Therefore the target polarization in the CM frame is

$$\begin{aligned} P_x &= P_T \sin\theta_T \cos(\phi_T - \phi_\pi), \\ P_y &= P_T \sin\theta_T \sin(\phi_T - \phi_\pi), \\ P_z &= \gamma_{CM}(p_T \cos(\theta_T) - \beta_{CM}) \end{aligned} \tag{12}$$

Note that if $\theta_T = 0$ the CM polarization is longitudinal, but if $\theta_T = 90^\circ$ there is still a longitudinal target polarization component in the CM system. In order to have a transversely polarized target in the CM system one has to choose $cos(\theta_T) = \beta_{CM}/P_T$. As an example for p_T =0.90 and a photon energy of 155 MeV, $\theta_T = 80.9^0$, a significant deviation from $\theta_T = 90^\circ$. As can be seen from Eq. 13 it is possible to produce a longitudinal target by pointing the target polarization in the beam direction. For the transverse polarization components another ϕ_π dependence is introduced.

Experimentally one usually measures asymmetries, which are generally obtained with more accuracy since they are less sensitive to normalizations than absolute cross sections. The seven asymmetries that can be obtained from the eight response functions are presented in Table 2. Here we introduce a new, more transparent notation as well as giving the historical one.

There are eight response functions in Eq. 11 but only six of them are independent[73, 74]. At each pion emission angle there are four complex invariant amplitudes[73, 74]. Taking into account the fact that one overall phase is irrelevant, this makes seven real numbers to determine experimentally in a complete experiment (i.e one in which all of the amplitudes are determined experimentally). Since an experiment with fully polarized photons and targets can only determine six of them, one must perform at least one more experiment in which the polarization of the recoil nucleon is measured in order to perform a complete experiment[73, 74].

There is also the important issue of how many partial waves are contributing. In the low energy regime one usually assumes that only the s and p wave multipoles are important. If one assumes this, then the angular distributions of all of the observables are limited; e.g. $\sigma_T = A_T + B_T \cos\theta + C_T \cos^2\theta$. If d waves become sufficiently important then $\sigma_T = A_T + B_T \cos\theta + C_T \cos^2\theta + D_T \cos^3\theta$. In addition to the greater angular variation when d waves are important, the numerical values of A_T, B_T, C_T are not the same. This simple example indicates the need to cover a sufficient angular range in each experiment and also sets requirements for the angular resolution and binning of the experiments. In general one must make reasonable (but model dependent) estimates of the contributions of the higher partial waves which contribute in order to make sure that significant contributions are not being overlooked.

We shall conclude this section by giving an example of how the multipoles have been extracted from the data at low energies. In the low energy region

Observable		Response Function	Name
$\sigma_T(\theta^*_\pi)$	=	$(p^*_\pi/p^*_\gamma)R^{00}_T$	Transverse Differential Cross Section
$A(\vec{\gamma}) \equiv \Sigma(\theta)$	=	$-R^{00}_{TT}/R^{00}_T$	Polarized Photon Asymmetry
$\boldsymbol{A(y) \equiv T(\theta)}$	=	$\boldsymbol{R^{0y}_T/R^{00}_T}$	Polarized Target Asymmetry
$A(\gamma_c, z) \equiv E(\theta)$	=	$-R^{0z}_{TT'}/R^{00}_T$	Circ. Photon- Long. Target
$A(\gamma_c, x) \equiv F(\theta)$	=	$R^{0x}_{TT'}/R^{00}_T$	Circ. Photon - Trans. Target
$\boldsymbol{A(\vec{\gamma}, z) \equiv G(\theta)}$	=	$\boldsymbol{-R^{0z}_{TT}/R^{00}_T}$	Trans. Photon - Long. Target
$\boldsymbol{A(\vec{\gamma}, x) \equiv H(\theta)}$	=	$\boldsymbol{R^{0x}_{TT}/R^{00}_T}$	Trans. Photon - Trans. Target
$\boldsymbol{A(\vec{\gamma}, y) \equiv P(\theta)}$	=	$\boldsymbol{-R^{0y}_{TT}/R^{00}_T}$	Trans. Photon - Normal Target

Table 2: Observables for photo-pion production [72] with polarized photons and targets. The top line is the unpolarized cross section. All other entries are asymmetries. The second box contains the single polarization observables. The next group consists of the double polarization observables. The last entry can also be observed as the recoil polarization asymmetry. A new, more transparent notation is introduced here for the asymmetries (e.g. $\boldsymbol{A(\vec{\gamma}, y)}$), and the historical notation (e.g. $\boldsymbol{P(\theta)}$) is also presented. As throughout this proposal, the time-reversal-odd observables (imaginary bilinear combinations of multipoles) are indicated with boldface. Only six of the eight observables are independent [73, 74].

(below $\simeq$ 165 MeV) it has been assumed that only s and p wave multipoles contribute and furthermore that the three p wave multipoles are purely real (see e.g.[24, 25, 26]). In this approximation (which must be checked with more accurate, future data) five numbers must be determined, $ReE_{0+}, ImE_{0+}, P_1, P_2$, and P_3, where these three P-wave amplitudes are defined in terms of the usual multipole amplitudes by:

$$\begin{aligned} P_1 &= 3E_{1+} + M_{1+} - M_{1-} \\ P_2 &= 3E_{1+} - M_{1+} + M_{1-} \\ P_3 &= 2M_{1+} + M_{1-} \ , \end{aligned} \tag{13}$$

where M_{1+} and M_{1-} are the P-wave magnetic dipole amplitudes for $j = \frac{3}{2}$ and $\frac{1}{2}$, respectively, and E_{1+} is the P-wave electric quadrapole amplitude with $j = \frac{3}{2}$ [60]. From the measurement of σ_T one obtains $A_T = \mid E_{0+} \mid^2 + 1/2(\mid P_2 \mid^2 + \mid P_3 \mid^2), B_T = 2Re(E_{0+}P_1^*)$, and $C_T = \mid P_1 \mid^2 - 1/2(\mid P_2 \mid^2 + \mid P_3 \mid^2)$. The next step was taken at Mainz by the measurement of the polarized photon asymmetry[26] which determines $R^{00}_{TT} = 1/2(\mid P_2 \mid^2 - \mid P_3 \mid^2)\sin(\theta)^2$. This still leaves us one observable short of an experimental determination of all of the multipoles, even with the restricted assumptions. The observable of choice is the time reversal odd polarized target asymmetry $\mathbf{R^{0y}_T} = Im[E_{0+}(P_3 - P_2)]\sin(\theta)$ (assuming real P-amplitudes) from which we can obtain ImE_{0+}. It should be noted that if there is a contribution from higher partial waves or if the imaginary parts of the p wave multipoles are not negligible then there will be additional θ

dependent terms in $\mathbf{R_T^{0y}}$. This can be experimentally tested with new data.

There are also two time reversal even asymmetries which are very large in the threshold region which can provide additional and precise measurements of the multipoles which will further test the assumptions on which the present data are analyzed. There are the two double polarization asymmetries induced with circular polarized photons $A(\gamma_c, z) \equiv E(\theta)$ and $A(\gamma_c, x) \equiv F(\theta)$. The numerator of the latter is $R^{0x}_{TT'} = \sin\theta Re[(E^*_{0+} + \cos\theta P^*_1)(P_2 - P_3)]$. It can be seen that a measurement of the angle (θ_0, not 0 or 180°) for which this observable = 0 provides an independent determination of $Re(E^*_{0+}) = -\cos\theta_0 Re(P_1)$. The full formulas for the observables are provided in the appendix.

5 Photo-Pion Production From the Nucleon

5.1 Previous $\gamma p \to \pi^0 p$ Experiments: Comparison With Theory

The observables that are most sensitive to the spontaneous hiding (breaking) of chiral symmetry in QCD are those that vanish in the chiral limit (light quark masses, or $m_\pi \to 0$). In πN physics these include the $a(\pi N)$: the s-wave πN scattering and charge exchange scattering lengths [29, 30], and $E_{0+}(\gamma^* N \to \pi^0 N)$: the electric dipole amplitude for electromagnetic π^0 production on the proton and neutron for real and virtual photons [18, 19, 20, 21]. In these cases the entire amplitude arises from the contributions of the small but finite quark (pion) masses and their momenta (assumed to be small) calculated in ChPT [16, 17]. A comparison of theory and experiment constitutes a low energy test of QCD and its symmetry properties, assuming the accuracy of ChPT. In the near future we expect that lattice calculations will begin to play a role. Therefore recent experiments have focused on observables that vanish in the chiral limit [28]. In the case of photo-pion production this means the $\gamma p \to \pi^0 p$ reaction. In the future we anticipate that with the use of deuteron targets this will also include the accurate measurement of the $\gamma n \to \pi^0 n$ reaction. As will be shown, the experiments for the unpolarized cross sections have reached a reasonable state of accuracy and there is good agreement between the one loop ChPT calculations and experiment. However further accuracy in the measurements of the unpolarized cross sections are anticipated in the near future and we are just at the beginning of experiments making extensive use of polarization degrees of freedom. These will provide far more stringent tests of the ChPT calculations.

Threshold photoproduction experiments with high-duty-cycle accelerators have been carried out at Mainz [24, 26] and Saskatoon [27]. In general, there is very reasonable agreement between the Mainz and Saskatoon data, and, for brevity, only the latest Mainz results [26] will be presented. These data cover the energy region from just above threshold (144.7 MeV) to 166 MeV in $\simeq 1$ MeV bins with tagged photons. The cross-section results for the energy region from threshold to 154 MeV are shown in Fig. 5. The agreement with the O(p^4) ChPT curves [21] is excellent and will be discussed below. The agreement of

the ChPT calculations with the differential cross section data up to 166 MeV is equally good.

The latest Mainz data [26] include the first use of linearly polarized photons in the threshold region for the $\gamma p \to \pi^0 p$ reaction. For statistical reasons, the entire energy range from threshold to 165 MeV was combined at the cross-section weighted average energy of 159.5 MeV. These data are shown in Fig. 6. There are two ChPT calculations that are being compared to the experiments. The older ChPT calculation [18, 19, 20] was carried out to $O(p^4)$ in the s-wave and to $O(p^3)$ in the p-wave multipoles. It has three empirically-determined counter terms, two in the s-wave and one in the p-wave multipoles. These were fit to the older Mainz and Saskatoon data [24, 25, 27], which only measured the unpolarized cross section. This meant that $\mathrm{Re}E_{0+}$ and two linear combinations of the p-wave multipoles were determined. The newer Mainz data [26] contain one average measurement of the linear photon asymmetry, which determines the third p-wave multipole at 159.5 MeV. Following this measurement, the ChPT calculations improved by also bringing the p-wave calculation to $O(p^4)$, consistent with the older s-wave calculation [21]; this marks the completion of the full one-loop calculation. In this calculation, there are now two more p-wave low-energy parameters which must be determined empirically. This was done by fitting to the new Mainz data. The resulting calculation gives the same curve as the empirical fit to the data(labeled fit). The improvement between the older and newer ChPT is also easily seen. It should be pointed out that the measurement of $A(\vec{\gamma}) \equiv \Sigma(\theta)$ is a very sensitive test of the theoretical calculations. Most models give the wrong sign for this quantity. Even dispersion relations predictions are not in agreement with the data (Fig. 6) indicating a deficiency in the data base on which this prediction is based.

At this point, there is impressive agreement between the data and the new, full, one-loop $O(p^4)$ ChPT calculations [21](see Figs. 1, 5, and 6). However concerns about how well the ChPT series is converging have been expressed for E_{0+}[18]. At $O(p^4)$ the p wave multipoles also showed that there were some significant effects ($\simeq 25\%$) which are almost cancelled out by a Δ contribution. These calculations were performed in the framework of Heavy Baryon ChPT (HBChPT) [18, 21]. Some open theoretical issues include the use of the relativistic ChPT[75], which might provide superior convergence. In addition there is the issue of the inclusion of the Δ as an active degree of freedom in ChPT calculations. To effectively carry out these calculations to higher order it may be useful to combine ChPT with dispersion relations. Some starts in this direction have been made. For example the most accurate calculation for Re E_{0+} have been made with relativistic ChPT combined with the Fubini-Furlan-Rosetti sum rule [51]. Finally, there is the issue of the upper limit to which this effective field theory is accurate. It is important to have experiments to explore the limits and see at what point theory and experiment diverge. For all of these reasons, it is important to extend the accurate tests of the theory to include more sensitive polarization observables which are more sensitive to the details of the theoretical predictions. Plans for the future will be discussed in Sec.5.2.

In addition to ChPT calculations there are many models of pion photopro-

duction, including MAID[76], a unitary-isobar model that is primarily designed to provide flexible fits of the data in the Δ and N^* regions, as well as other dynamical models [77, 78]. However, in the near-threshold region, MAID or the other dynamical model calculations do not agree very well with the existing data. The DMT (Dubna-Mainz-Tapei) dynamical model is an extension of MAID and has proven to be more accurate in the near-threshold region [50]. This can be used to estimate the magnitude of the Δ contribution which increases rapidly with photon energy and provides a planning tool for projected experiments and for comparison with future data. In addition there is the empirical SAID multipole analysis of the existing data [79].

5.2 Future $\vec{\gamma}\vec{p} \to \pi^0 p$ Experiments

In this section we present the physics that can be obtained from precise measurements of photo-pion production from the proton from threshold to intermediate energies below the Δ resonance. The emphasis is on the open questions, keeping in mind the experimental capabilities that presently exist or are in an active stage of development. In Section 3, we have presented an overview of the unique capabilities at HIγS and Mainz to perform $\vec{\gamma}\vec{p} \to \pi^0 p,\ \pi^+ n$ experiments with beam and target polarizations. These two facilities provide complementary capabilities. At Mainz the experiments will be carried out with tagged-photons in which a range of photon energies and pion angles will be measured simultaneously. At HIγS, the plan is to measure both charge channels at several photon energies with high statistics.

The data up to a photon energy of $\simeq 165$ MeV will provide a stringent test of the one-loop ChPT calculations [21] as well as a measure of the energies at which they do not accurately converge. The data will include both charge channels and a determination of the energy dependence of all of the s- and p-wave multipoles for the first time. These experiments are well within the capabilities outlined in Sec. 3. They should include a precise measurement of the unitary cusp in the region of the $\pi^+ n$ threshold at 151.4 MeV. They should provide a first measurement of the π-N phase shifts in the neutral channels. This includes a measurement of the s-wave charge exchange scattering length $a_{cex}(\pi^+ n \to \pi^0 p)$, which will be a measure of isospin symmetry in the πN system at the few % level.

First we show the order of magnitude expected for the observables. The cross sections have been shown in Fig. 5. It is seen that the $O(p^4)$ ChPT calculations[21] are in excellent agreement with experiment. However the experiments using polarization have just barely begun. These are needed to stringently test the theory. Using transversely polarized photons and unpolarized targets, one can access $A(\vec{\gamma}) \equiv \Sigma(\theta) = -R_{TT}/R_T$. This is the smallest of the three time-reversal-even asymmetries. A first measurement of this quantity has been performed at Mainz [26] and the results are shown in Fig. 6 and discussed in the previous subsection(5.1). This observable is important for determining the p-wave amplitudes and is a significant test of ChPT calculations [18, 19, 20, 21]. In the future a measurement of the energy dependence of this quantity can be

performed. A full MonteCarlo simulation was performed for the anticipated experiments at HIγS. The predictions of ChPT were used for the $\pi^0 p$ channel, while those of the DMT model were employed in the case of the $\pi^+ n$ channel. The experimental setup utilized the Crystal Box assembly described in Sec. 3 for π^0 detection and the Blowfish neutron detector array, arranged in a 9×9 assembly (with a center opening) for neutron detection. The beam-on-target intensity was taken to be 10^7 γ/s, and the HIFROST target was assumed with a thickness of 3.5×10^{23} protons/cm^2. All observables were measured at all CM scattering angles. The observables for the case of the π^0p channel which were considered were $\sigma_T(\theta)$, $\Sigma(\theta)$, $T(\theta)$, $E(\theta)$, and $F(\theta)$. The same was true for the π^+n channel, except that T(θ), which is negligibly small in this channel, was omitted.

The projected observables for the π^0p channel are shown in Fig. 7. The estimated single-polarization asymmetries at 90 degrees as a function of photon energy are shown in the upper panels of Fig. 7. Note that $A(\gamma) \equiv \Sigma(90^\circ)$ is non-zero starting at the $\pi^0 p$ threshold, since it depends on the p-wave amplitudes, which rise smoothly with energy. The plotted points show the estimated errors that will be obtained in runs of $\simeq$ 100 hours each at HIγS. Similar errors can be obtained at Mainz, although with longer running times.

As can be seen in the upper right panel of Fig. 7 the curves for $\boldsymbol{A(y) \equiv T(90^\circ)}$ rise rapidly at the $\pi^+ n$ threshold. This is because it is proportional to Im E_{0+} which rises rapidly at that threshold due to the unitary cusp. The two curves show the large difference in Im E_{0+} for the unitary [42] ($\beta = 3.43$) and ChPT [18, 19, 20, 21] calculations ($\beta = 2.78$) discussed in Sec. 2.2 and shown in Fig. 1. These curves show the sensitivity to β that will enable us to measure $a_{cex}(\pi^+ n \to \pi^0 p)$.

Predictions for the two time-reversal-even asymmetries $A(\gamma_c, z) \equiv E(90^\circ)$ and $A(\gamma_c, x) \equiv F(90^\circ)$ are presented in the lower panels of Fig. 7. These involve circularly polarized photons and polarized targets. Their values are predicted to be quite large and show the cusp structure in the s-wave production amplitude E_{0+} due to the presence of $\mid E_{0+} \mid^2$ and the interference of ReE_{0+} with the p-wave amplitudes. Both of these observables contain a different sensitivity to the s- and p-wave multipoles in comparison with the unpolarized cross section.

These will be the first measurements of the imaginary part of E_{0+}. The errors that we anticipate for E_{0+} are shown in Fig. 1. These errors are based upon the assumption that we measure all four observables shown in Fig. 7 at each energy and all CM angles. For the real part the significant improvement over what has been previously achieved is evident. Among other issues the convergence of the ChPT series in photon energy will be tested by these experiments.

The observables of Fig. 7 also lead to values for the three p-waves amplitudes. The results are shown in Fig. 8, along with to the predictions of ChPT [18, 19, 20, 21]. Note that although there has been a previous report for the (small) value of Re $E_{1+}^{\pi^\circ p}$ [58], but it is highly model dependent since it relies on a measurement of coherent π^0 photoproduction in Carbon. This will be the first model independent determination of this small multpole including is energy

dependence and will provide a very sensitive test of the predictions of ChPT.

Last, but far from least, we discuss one case in which isospin breaking is $\simeq (m_d - m_u)/(m_d + m_u) \simeq 25\%$ rather then the usual $\simeq (m_d - m_u)/\Lambda_{QCD} \simeq 2\%$. The quantity of interest is $a(\pi^0 p)$, the s-wave π^0 scattering length on the proton [30, 31]. Clearly this quantity cannot be directly measured since π^0 beams cannot be constructed. Our present knowledge comes from data involving charged pions and constructing the isospin even s-wave scattering length $a^+ = (a_{\pi^- p} + a_{\pi^+ p})/2 = (a_{\pi^- p} + a_{\pi^- n})/2$ (it is understood that the Coulomb contributions have been removed). This can be obtained from scattering data or more accurately from pionic hydrogen and deuterium [34, 33]. If isospin symmetry holds, then $a^+ = a(\pi^0 p)$. In analyzing the pionic hydrogen and deuterium data it has been shown that the isospin breaking terms, which are primarily electromagnetic in origin, have to be taken into account [34]. When this is done, the latest reported data give the value $a^+ = (0.0069 \pm 0.0034) m_\pi^{-1}$ [33].

It has been suggested that $a(\pi^0 p)$ can be measured as a final state interaction in the $\gamma\vec{p} \to \pi^0 p$ reaction with transversely polarized protons in the energy region between the π^0 threshold of 144.7 MeV and the π^+ threshold of 151.4 MeV [42]. The HIγS facility may be capable of a direct measure of this provided that it can produce a beam $\simeq 10^9$ photons/s on target. A 1000 hour experiment will enable a measurement of $a(\pi^0 p)$ with a statistical accuracy $\simeq 10^{-3}/m_\pi$, which is comparable with the present determination of a^+. A comparison of $a(\pi^0 p)$ and a^+ will test the predicted violation of isospin symmetry by $\simeq 25\%$ [30, 31].

5.3 The $\vec{\gamma}\vec{p} \to \pi^+ n$ Reaction

For charged pion photoproduction there is the low-energy theorem of Kroll and Ruderman [10] which leads to an electric dipole amplitude ratio $E_{0+}(\gamma p \to \pi^+ n)/E_{0+}(\gamma p \to \pi^0 p) \simeq$ -20. Both the magnitude and sign of this ratio is observable in a unitary cusp which is most visible in the π^0 channel, the strength of which is characterized by the parameter $\beta = E_{0+}(\gamma p \to \pi^+ n) a_{cex}(\pi^+ n \to \pi^0 p)$ (see Sec. 2.2).

There is only one modern $\gamma p \to \pi^+ n$ experiment in the near-threshold region [48]. This was performed at Saskatoon by neutron detection yielding the threshold value $E_{0+}(\gamma p \to \pi^+ n) = (28.06 \pm 0.27 \pm 0.45) \times 10^{-3}/m_{\pi^+}$ where the first error is statistical and the second is systematic. This is in good agreement with the predictions of the Kroll-Ruderman term plus the chiral corrections [49] of 28.2 ± 0.6 using the "old" value of the πN coupling constant $f_{\pi N}^2 = 0.079 \pm 0.002$ (2.1%). Since the dominant Kroll-Ruderman term is proportional to $f_{\pi N}$, the experimental value of E_{0+} can be used to extract the value of $f_{\pi N}^2 = 0.078 \pm 0.004$, where the total experimental and theoretical errors are added in quadrature. This is part way between the old value and the newer value of $f_{\pi N}^2 = 0.075 \pm 0.001$ [80], but the error is too large to distinguish between these two values. In addition we note that the dispersion analysis [81] gives a value of $E_{0+}(\gamma p \to \pi^+ n)$ of 28.0 ± 0.2 (0.7% lower) which is significant for this purpose. It is clear that an improvement in accuracy for both the theory

and experiment are important to obtain an independent, accurate value for the πN coupling constant (for further discussion see [82]).

As was discussed above a major motivation to measure $E_{0+}(\gamma p \rightarrow \pi^+ n)$ accurately is that it is needed to extract the value of $a_{cex}(\pi^+ n \rightarrow \pi^0 p)$ from the value of β measured in neutral pion photoproduction [42, 45] (see Sec. 2.2). A realistic goal for an accuracy of $\simeq 2\%$ is sufficient for the first round of experiments but it would ultimately need to be improved to reach the $\leq 1\%$ requirement for isospin tests. In addition, there is considerable interest in exploring the energy dependence of $E_{0+}(\gamma p \rightarrow \pi^+ n)$ in order to test the chiral corrections to the Kroll-Ruderman theorem and which also affect the energy dependence of the β parameter in π^0 production. Furthermore, it would be of considerable interest to measure the p-wave multipoles to further test the ChPT calculations [21] in this channel. Both of these measurements will require full polarization, since both the p-wave multipoles and the chiral corrections to the Kroll-Ruderman theorem are relatively small. The differential cross sections for the $\gamma p \rightarrow \pi^0 p$, $\pi^+ n$ reactions at a photon energy of 164 MeV are shown in Fig. 9. The projected statistical errors in the data points shown are based on running for 100 hours at HIγS for each data point using the experimental setup at HIγS.

Figure 9 also displays the results of our MonteCarlo simulation for the polarization observables $\Sigma(90^\circ)$, $E(90^\circ)$, and $F(90^\circ)$ as a function of γ-ray energy for the $\pi^+ n$ channel. These projected results are based on the DMT model. Notice that while $\Sigma(90^\circ)$ is much smaller here than in the $\pi^0 p$ channel, the $E(90^\circ)$ and $F(90^\circ)$ values are considerable.

The results of measuring the four observables shown in Fig. 9 at essentially all CM angles (there are slight losses at extreme angles) lead to values for the Re E_{0+} in the $\pi^+ n$ channel, as shown in Fig. 10. This result, when combined with the value of β obtained in the π^0p experiment, will lead to an accurate value of $\mathrm{a}_{cex}(\pi + n \rightarrow \pi^0 p)$ (see Eq. 4) as well as the value of $f_{\pi n}$, the pion-nucleon coupling constant. It can be seen that the charged-pion cross sections are over 20 times larger than for neutral pion production. This is a consequence of the large Kroll-Ruderman term [10, 49], which enhances the s-wave amplitude E_{0+} for charged pions. Another consequence of this is that π^0 production is p-wave-dominated at these energies. This can be seen from the fact that the differential cross section varies more rapidly with angle for the neutral pion production than for the $\pi^+ n$ channel.

5.4 Photo-Pion Production From the Neutron: Charge Symmetry Tests

To properly study photo-pion production from the nucleon we also need to consider the $\vec{\gamma}\vec{n} \rightarrow \pi^0 n, \pi^- p$ reactions. There are four charge channels, and assuming that isospin is conserved for the strong interactions (i.e. for the final πN states), there are three independent isospin amplitudes for each multipole [73]. Therefore to completely determine these multipoles experimentally it takes a complete experiment on three of the charge channels. To test isospin conserva-

tion it will take a similar experiment on the fourth charge channel. In order to do this in a significant way one would need to determine the multipoles at the 1% level.

The most straightforward approach to measuring the four reaction channels is to consider the deuteron as a target. This introduces few body physics which must be shown to be under control in order to extract accurate neutron target data. On the other hand it provides additional important physics such as testing effective field theory calculations for the two body system. An important first step in the theory has been taken by the $O(p^4)$ ChPT calculation of the coherent $\gamma D \to \pi^0 D$ reaction at threshold and its demonstration that the neutron-π^0 contribution is significant [84]. The use of the deuteron target also allows the study of the charge symmetry of the NN interaction at low energies [85] which is also fundamental since any charge asymmetry is due in part to the up, down quark mass difference.

One channel which involves the neutron, but not the deuteron, is the "inverse" $\pi^- p \to \gamma n$ reaction for which there is some data from TRIUMF between threshold and the Δ resonance [86, 87]. On the theoretical side there is an $O(p^3)$ ChPT calculation [88] which is in reasonable agreement with all of the data [86]. Furthermore it should be noted that if the assumption of resonance saturation is employed in ChPT calculations, the low energy parameters derived from the proton data can be used to predict the two charge channels on the neutron [18]. Clearly the photopion amplitudes from the neutron are as fundamental as those for the proton, just more difficult to access experimentally. This is a future challenge for the field.

Few body calculations for the deuteron can be tested for many reactions such as $\gamma D \to \pi^0 D, \pi^0 np, \pi^+ nn, \pi^- pp$. In addition there are special kinematic regions where the two outgoing nucleons move together with a small relative momentum. It is this regime that is very sensitive to the a_{NN}: the three nucleon-nucleon scattering lengths. There is a long history of measurements and calculations on this subject (for a review see [89]). It has been concluded that there is strong evidence for a charge symmetry violation because $a_{nn} - a_{pp}$ is not equal to zero [89]. However there has been a long controversy over the value of a_{nn}. Many of the reactions used to measure this quantity have three interacting hadrons in the final state. The radiative capture reaction $\pi^- p \to nn\gamma$ does not have this problem and an accurate value of a_{nn} has been extracted using it [90]. It has been shown by accurate modern calculations that the $\gamma D \to nn\pi^+$ reaction should also be capable of obtaining an accurate value [85]. This reaction has the advantage that there are certain ranges of the kinematic parameters that are insensitive to a_{nn} and which therefore can be used to test the reaction calculations. In addition the two other reactions $\gamma D \to \pi^0 np, \pi^- pp$ can be used to measure a_{np} and a_{pp} which have previously been accurately measured [89]. This will provide a strict test of this method. Accurate data on the three N-N scattering lengths are another way to get at the isospin breaking dynamics due to the mass difference of the up and down quarks [91].

6 Conclusions

We have described a significant program of photo-pion physics that can be carried out at the HIγS facility and at Mainz. Specifically, we can achieve the following:

- A first full measurement of the unitary cusp in the real and imaginary parts of the s-wave electric dipole amplitude $E_{0+}(\gamma p \to \pi^0 p)$ from a measurement of the transverse polarized target asymmetry $\boldsymbol{A(y) = T(\theta)}$. This will provide the energy dependence of ImE_{0+} and an accurate measurement of $\beta = E_{0+}(\gamma p \to \pi^+ n) a_{cex}(\pi^+ n \to \pi^0 p)$. With our value of $E_{0+}(\gamma p \to \pi^+ n)$, we will obtain a first measurement of $a_{cex}(\pi^+ n \to \pi^0 p)$ at the few % level of accuracy. As has been discussed in Sec. 2.2, this will be a test of isospin breaking, which has been predicted due to the mass difference of the up and down quarks $m_d - m_u$.

- The first measurement of the energy dependence of $A(\gamma) \equiv \Sigma(\theta)$ for the $\gamma p \to \pi^0 p$ reaction. Combined with accurate cross-section measurements [26] this will enable us to obtain the energy dependence of the three p-wave multipoles, which will test the theoretical calculations [21, 50, 83].

- We have shown that there is a realistic possibility to measure $a(\pi^0 p)$, the s-wave π^0 scattering length on the proton, as a final state interaction in the $\gamma \vec{p} \to \pi^0 p$ reaction with transversely polarized protons in the energy region between the π^0 threshold of 144.7MeV and the π^+ threshold of 151.4 MeV[42] to a state-of-the-art accuracy of $\simeq 10^{-3}/m_\pi$. This quantity is predicted to have an isospin breaking $\simeq (m_d - m_u)/(m_d + m_u) \simeq 25\%$ rather then the usual $\simeq (m_d - m_u)/\Lambda_{QCD} \simeq 2\%$[30, 31].

- A more accurate measurement of the cross section for the $\gamma p \to \pi^+ n$ reaction just above threshold. From this, we can obtain a more accurate value (1-to-2 %) for $E_{0+}(\gamma p \to \pi^+ n)$ and the πN coupling constant ($f^2_{\pi N}$) at the same level of accuracy, as well as $a_{cex}(\pi^+ n \to \pi^0 p)$, as discussed above.

- A first measurement of the asymmetries in the $\gamma p \to \pi^+ n$ reaction just above threshold. Combined with the accurate measurement of $E_{0+}(\gamma p \to \pi^+ n)$, this will enable us to obtain the p-wave multipoles in this channel for the first time. This can be used as a further test of the theoretical calculations [21, 50, 83].

- The measurement of π N scattering lengths, and the possible checking of a large isospin breaking at intermediate energies, indicates the sensitivity of photo pion reactions to the pion-nucleon final state when transversely polarized targets are employed. This shows the ability to measure π N phase shifts in states with a minimum electromagnetic interaction.

These experiments for the $\vec{\gamma}\vec{p} \to \pi^0 p$, $\pi^+ n$ reactions with photon energies just above the $\pi^+ n$ threshold (151.4 MeV) up to $\simeq$ 160 MeV are planned for

near-term operation of the HIγS facility and at Mainz. The intermediate-energy isospin-breaking experiments discussed in Sec. 2.3 can be performed at Mainz and, as soon as the upgrades outlined in this paper have been completed, at the HIγS facility. We believe that these data will provide stringent new tests of ChPT, and probe the isospin breaking due to the mass difference of the up and down quarks.

7 Acknowledgments

The work described in this paper is supported in part by US Department of Energy, Office of Science grants DE-FG02-97ER41033 and DE-FG02-94ER40818, and US Department of Defense MFEL Program contract number FA9550-04-01-0086. We would also like to thank V. Bernard, U.G. Meissner, and C. Fernandez-Ramirez for their comments on the manuscript and discussions.

A s- and p-Wave Multipole Expansion of the Response Functions

For convenience we have collected the formulas for some of the response functions in terms of the s and p wave multipole amplitudes starting with the time reversal even (RE) observables: The A_T, B_T, C_T coefficients of σ_T and the polarized photon(unpolarized target) responses are:

$$\begin{array}{c} R_T(\theta) = A_T + B_T \cos\theta + C_T \cos^2\theta \\ A_T = |E_{0+}|^2 + |P_{23}^+|^2 \\ B_T = 2Re(E_{0+}P_1^\star) \\ C_T = \mid P_1|^2 - |P_{23}^+|^2 \\ R_{TT} = \sin^2\theta |P_{23}^-|^2 \end{array} \tag{14}$$

Here we ave introduced the ChPT notation for the p wave multipoles:

$$\begin{array}{c} P_1 = 3E_{1+} + M_{1+} - M_{1-} \\ P_2 = 3E_{1+} - M_{1+} + M_{1-} \\ P_3 = 2M_{1+} + M_{1-} \\ |P_{23}^\pm|^2 = (|P_2|^2 \pm |P_3|^2)/2 \end{array} \tag{15}$$

$$\begin{array}{c} R_{TT'}^{0z} = a_{TT'}^{0z} + b_{TT'}^{0z}\cos\theta + c_{TT'}^{0z}\cos^2\theta \\ a_{TT'}^{0z} = -|E_{0+}|^2 - Re(P_2^* P_3) \\ b_{TT'}^{0z} = -2Re(E_{0+}^* P_1) \\ c_{TT'}^{0z} = Re(P_3^* P_2) - |P_1|^2 \end{array} \tag{16}$$

$$R_{TT'}^{0x} = \sin\theta Re[(E_{0+}^* + \cos\theta P_1^*)(P_2 - P_3)] \tag{17}$$

For the largest time reversal odd observable

$$R_T^{0y} = \sin\theta Im[((E_{0+}^* + \cos\theta P_1^*)(P_2 - P_3)] \tag{18}$$

Note that this is the imaginary amplitude of $R^{0x}_{TT'}$.

These all can be derived from the complete formulas using the CGLN F invariant amplitudes expanded into s and p waves[72].

$$\begin{gathered} F_1 = E_{0+} + 3(M_{1+} + E_{1+})\cos\theta = E_{0+} + (P_1 + P_3)\cos\theta \\ F_2 = M_{1-} + 2M_{1+} = P_3 \\ F_3 = 3(E_{1+} - M_{1+}) = P_2 - P_3 \\ F_4 = 0 \end{gathered} \tag{19}$$

References

[1] E. Amaldi, S. Fubini, and G. Furlan. Springer Tracts in Modern Physics, 83, 1979.

[2] Y. Nambu. Phys. Rev. Lett, 4:380, 1960.

[3] Y. Nambu and Jona-Lasinio. Phys. Rev., 122:345, 1961.

[4] Y. Nambu and Jona-Lasinio. Phys. Rev., 124:246, 1961.

[5] J.F.Donoghue, E.Golowich, and B.R.Holstein. Dynamics of the Standard Model. Cambridge University Press, 1992.

[6] P. de Baenst. Nucl. Phys., B24:633, 1970.

[7] A.I. Vainshtein and V.I. Zakharov. Sov. J. Nucl. Phys., 12:333, 1971.

[8] A.I. Vainshtein and V.I. Zakharov. Nucl. Phys., B36:589, 1972.

[9] G. Ecker and U.G. Meißner. Comm. Nucl. Part. Phys., 21:347, 1995.

[10] N.M. Kroll and M.A.Ruderman. Phys. Rev., 93:233, 1954.

[11] S. Weinberg. Physica, A96:327, 1979.

[12] J.Gasser and H.Leutwyler. Ann. Phys.(N.Y.), 158:142, 1984.

[13] J.Gasser and H.Leutwyler. Nucl.Phys., B250:465, 1985.

[14] J.Gasser and H.Leutwyler. Nucl.Phys., B250:517, 1985.

[15] M. W. Ahmed, B.R.Holstein, H. Gao, and H. R. Weller. Proceedings of the Workshop on Chiral Dynamics 2006:Theory and Experiment. World Scientific, 2007.

[16] V. Bernard and U.G. Meißner. Ann. Rev. Nucl. Part. Sci, 57:33, 2007.

[17] V. Bernard. Prog. Part. Nucl. Phys., 60:82, 2008.

[18] V. Bernard, N. Kaiser, and U. G. Meißner. Int. J. Mod. Phys., E4:193, 1995.

[19] V. Bernard, N. Kaiser, and U. G. Meißner. Nucl. Phys., B383:442, 1992.

[20] V. Bernard, N. Kaiser, and U. G. Meißner. Phys. Rev. Lett., 74:3752, 1995.

[21] V.Bernard, N.Kaiser, and U.G.Meissner. Eur. Phys. J., A11:209, 2001.

[22] V. Bernard et al. Phys. Lett., B268:291, 1954.

[23] V. Bernard et al. Z. Phys., C70:483, 1996.

[24] A. M. Bernstein et al. Phys. Rev., C55:1509, 1997.

[25] M. Fuchs et al. Phys. Lett., B368:20, 1996.

[26] A. Schmidt et al. Phys. Rev. Lett., 87:232501, 2001.

[27] J.C. Bergstrom et al. Phys. Rev., C53:R1052, 1996.

[28] M. W. Ahmed, B.R.Holstein, H. Gao, and H. R. Weller. See the article by A.M. Bernstein in Proceedings of the Workshop on Chiral Dynamics 2006:Theory and Experiment. World Scientific, 2007.

[29] S. Weinberg. Phys. Rev. Lett., 17:168, 1966.

[30] S. Weinberg. In Transactions of the N.Y.Academy of Science Series II, volume 38, page 185, 1977.

[31] N. Fettes and U.G.Meißner. Nucl. Phys., A693:693, 2001.

[32] N. Fettes and U.G.Meißner. Phys. Rev., C63:045201, 2001.

[33] D. Gotta. In AIP conf. Proc., volume 1037, page 162, 2008.

[34] U.G.Meißner et al. Phys. Lett., B639:478, 2006.

[35] U.G.Meißner et al. Eur. Phys. J., C41:213, 2005.

[36] V. Baru et al. arXiv:0711.2743.

[37] G. Lamanna. J. Phys. Conf. Ser, 110:022027, 2008.

[38] Gilberto Colangelo, Juerg Gasser, and Akaki Rusetsky. Eur. Phys. J. C, C59:75–98, 2009.

[39] Ulf-G. Meissner and S. Steininger. Phys. Lett., B419:403, 1998.

[40] W. R. Gibbs et al. Phys. Rev. Lett., 74:3740, 1995.

[41] E. Matsinos. Phys. Rev., C58:3014, 1997.

[42] A. M. Bernstein. Phys. Lett., B442:20, 1998.

[43] E. Fermi. Suppl. Nuovo Cimento, 2:17, 1955.

[44] K. M. Watson. Phys. Rev., 95:228, 1954.

[45] B. Ananthanarayan. Phys. Lett., B634:391, 2006.

[46] V. F. Grushin. In Proceedings of the Lebedev Physics Insitute, Academy of Ssciences of the USSR, A.A.Komar, editor, volume 186, 1988.

[47] V. Bernard, N. Kaiser, and Ulf.G. Meissner. Phys. Lett., B309:421, 1993.

[48] E. Korkmaz et al. Phys. Rev. Lett., 83:3609, 1999.

[49] V. Bernard, N. Kaiser, and U.-G. Meissner. Phys. Lett., B383:116, 1996.

[50] S.S. Kamalov et al. Phys. Lett., B522:27–36, 2001.

[51] Veronique Bernard, Bastian Kubis, and Ulf-G. Meissner. The Fubini-Furlan-Rosetti sum rule and related aspects in light of covariant baryon chiral perturbation theory. Eur. Phys. J., A25:419–425, 2005.

[52] Y. Jia et al. Phys. Rev. Lett., 101:102301, 2008.

[53] A. M Bernstein. PiN Newslett., 15:140–143, 1999.

[54] J. M . Vogt et al. Nucl. Inst. and Meth. in Phys. Res., A324:198–208, 1993.

[55] D. Lohmann et al. Nucl. Inst. and Meth. in Phys. Res., A343:494–507, 1994.

[56] J. M. Vogt et al. Nucl. Inst. and Meth. in Phys. Res., A366:100–114, 1995.

[57] J. M. Vogt et al. Nucl. Inst. and Meth. in Phys. Res., A324:198–208, 1993.

[58] J. C. Bergstrom et al. Phys. Rev., C55:2016, 1997.

[59] J. C. Bergstrom. Phys. Rev., C58:2574, 1998.

[60] J. C. Bergstrom et al. Phys. Rev., C57:3203, 1998.

[61] S. J. Hall et al. Nucl. Inst. and Meth. in Phys. Res., A368:698, 1996.

[62] I. Anthony et al. Nucl. Inst. and Meth. in Phys. Res., A301:230, 1991.

[63] A. R. Gabler et al. Nucl. Inst. and Meth. in Phys. Res., A346:168, 1994.

[64] V. N. Litvinenko. Phys. Lett., B78:4569, 1997.

[65] H. R. Weller et al. Prog. Part. Nucl. Phys., 62:257–303, 2009.

[66] R. D. Bolton et al. Phys. Rev., D38:2077, 1988.

[67] M. W. Ahmed et al. Phys. Rev., C68:064004, 2003.

[68] M. A. Blackston et al. Phys. Rev., C78:034003, 2008.

[69] T. O. Ninikoski. Nucl. Inst. and Meth., 134:219–233, 1976.

[70] H. Dutz. Nucl. Inst. and Meth. in Phys. Res., A356:111–115, 1995.

[71] M. Plückthun. Nucl. Inst. and Meth. in Phys. Res., A400:133–136, 1997.

[72] G. Knochlein, D. Drechsel, and L. Tiator. Z. Phys., A352:327–343, 1995.

[73] D. Drechsel and L.Tiator. Nucl, Part. Phys., 18:449, 1992.

[74] A. S. Raskin and T. W. Donnelly. Ann. of Phys.(N.Y.), 191:78, 1989.

[75] Thomas Becher and H. Leutwyler. Low energy analysis of pi N –¿ pi N. JHEP, 06:017, 2001.

[76] D. Drechsel et al. http://www.kph.uni-mainz.de/MAID/ and Nucl. Phys., A645:145, 1999.

[77] T. Sato and T. S. H. Lee. Dynamical study of the Delta excitation in N(e,e' pi) reactions. Phys. Rev., C63:055201, 2001.

[78] C. Fernandez-Ramirez, E. Moya de Guerra, and J. M. Udias. Effective Lagrangian approach to pion photoproduction from the nucleon. Annals Phys., 321:1408–1456, 2006.

[79] R. Arndt et al. http://gwdac.phys.gwu.edu/ and Phys. Rev., C66:055213, 2002.

[80] J. J. DeSawart et al.

[81] O. Hanstein, D. Dreschel, and L.Tiator. Phys. Lett., B399:13, 1997.

[82] A.M.Bernstein and N. Kaiser. Working group on electromagnetic production of Goldstone Bosons, Workshop on Chiral Dynamics: Theory and Experiment Mainz, Germany, Lecture Notes in Physics, 513, 1998.

[83] S.N. Yang et al. Nucl. Phys., A737:248–252, 2004.

[84] S. R. Beane, V. Bernard, T. S. H. Lee, Ulf-G. Meissner, and U. van Kolck. Neutral pion photoproduction on deuterium in baryon chiral perturbation theory to order q**4. Nucl. Phys., A618:381–401, 1997.

[85] V. Lensky et al. Eur. Phys .J, A33:339–348, 2007.

[86] A. Bagheri et al. THE REACTION pi- p → gamma n BELOW THE DELTA RESONANCE. Phys. Rev., C38:875–884, 1988.

[87] M. A. Kovash. Total cross-sections for pi- p → gamma n at 10-MeV to 20-MeV. PiN Newslett., 12N3:51–55, 1997.

[88] Harold W. Fearing, Thomas R. Hemmert, Randy Lewis, and Christine Unkmeir. Radiative pion capture by a nucleon. Phys. Rev., C62:054006, 2000.

[89] G. A. Miller, B. M. K. Nefkens, and I. Slaus. Charge symmetry, quarks and mesons. Phys. Rept., 194:1–116, 1990.

[90] A. Gardestig and D. R. Phillips. Using chiral perturbation theory to extract the neutron neutron scattering length from pi- d –¿ n n gamma. Phys. Rev., C73:014002, 2006.

[91] Markus Walzl, Ulf G. Meissner, and Evgeny Epelbaum. Charge-dependent nucleon nucleon potential from chiral effective field theory. Nucl. Phys., A693:663–692, 2001.

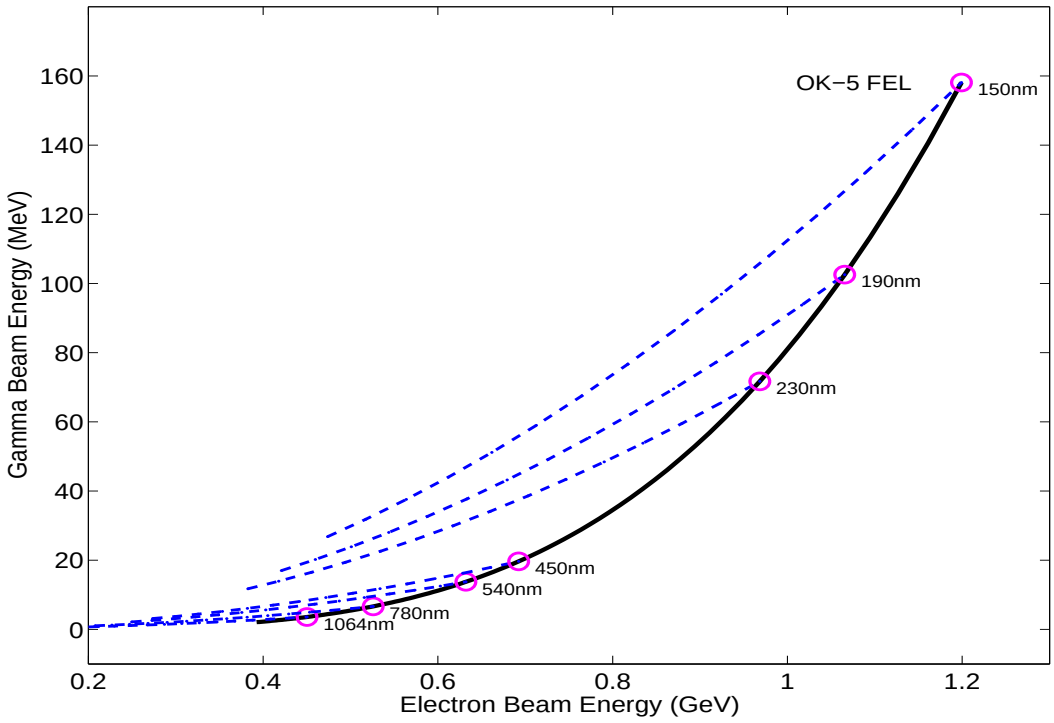

Figure 4: The energy tuning range of the circularly polarized γ-ray beam with the OK-5 FEL from 1064 nm down to 150 nm. A set of radiation resistive FEL mirrors with a high reflectivity at 150 nm are necessary to reach the highest gamma-beam energies – about 158 MeV with the existing 1.2 GeV storage ring. For a given FEL wavelength, the highest gamma energy is determined by the highest electron beam energy for FEL lasing as limited by the maximum magnetic field of the wigglers. The thick black curve shows the maximum gamma energy as a function of the electron beam energy by varying FEL wavelengths. The blue dashed curve show the gamma energy range for a fixed FEL wavelength.

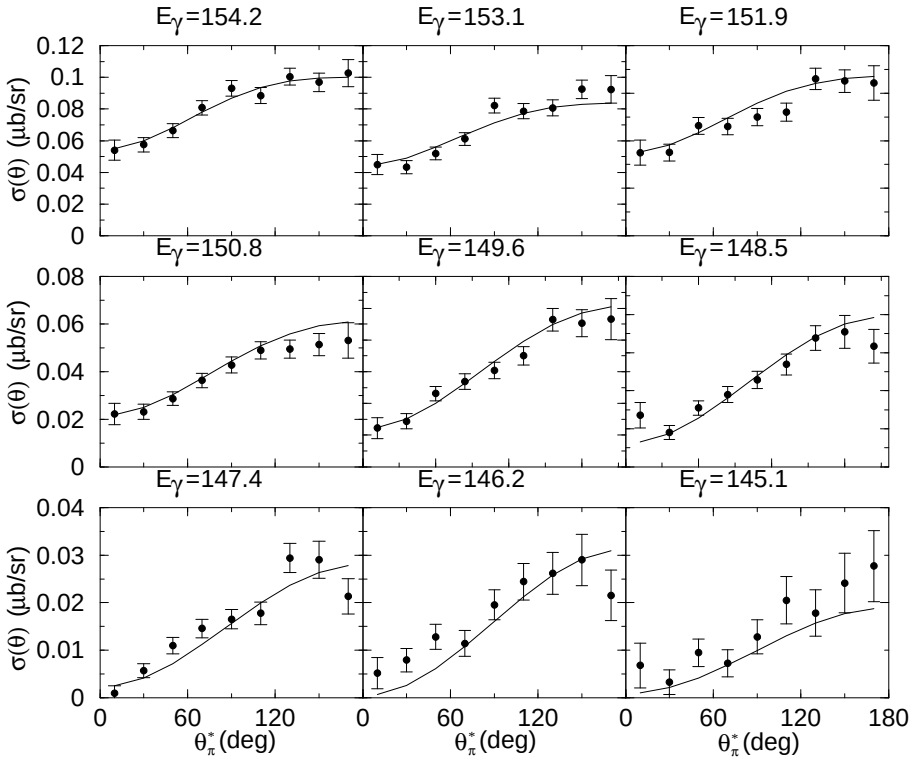

Figure 5: Experimental differential cross sections in μb/sr versus pion center-of-mass angle for the $\gamma p \to \pi^0 p$ reaction for a series of photon energies, labeled above each figure, starting just above threshold (144.7 MeV) [26]. The errors are statistical and do not include the 5 % systematic error. The curves are the latest O(p^4) ChPT calculation [21] fit to the data (see text for discussion).

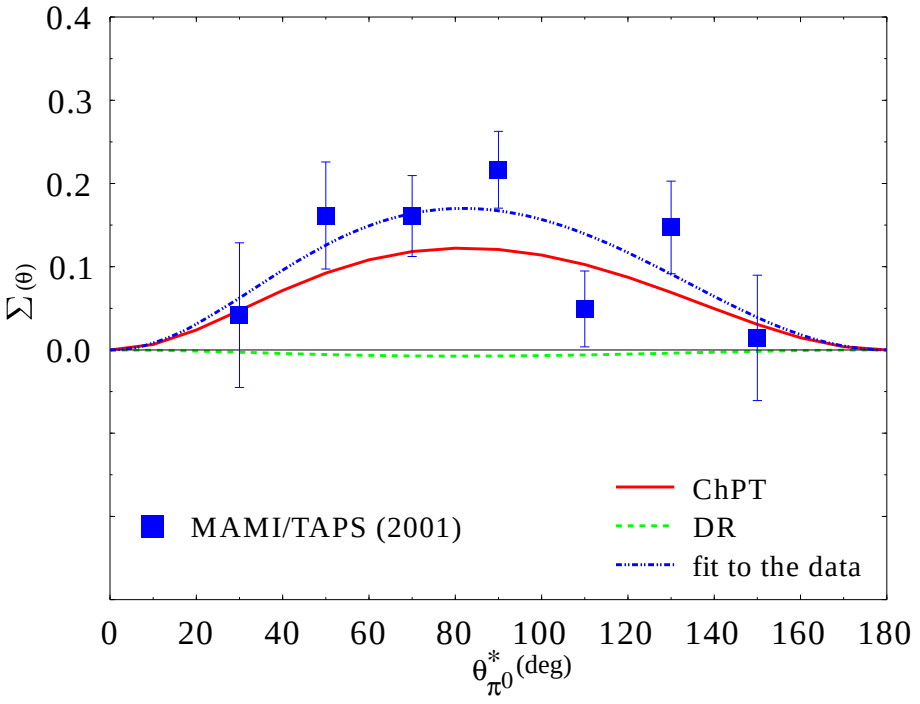

Figure 6: Experimental polarized photon asymmetry ($A(\vec{\gamma}) \equiv \Sigma(\theta)$) versus pion center-of-mass angle for the $\gamma p \to \pi^0 p$ reaction.These data are the cross section weighted asymmetries from threshold to 166 MeV at the average energy of 159.5 MeV [26]. The errors are statistical and do not include the 3% systematic error. The solid curve, labeled "ChPT," is an older [O(p^3)] ChPT calculation [18, 19, 20]. The curve with the small dots, labeled "fit to the data," is a fit to the data and also is the same as the newer [O(p^4)] ChPT calculation [21] with several new low energy parameters.

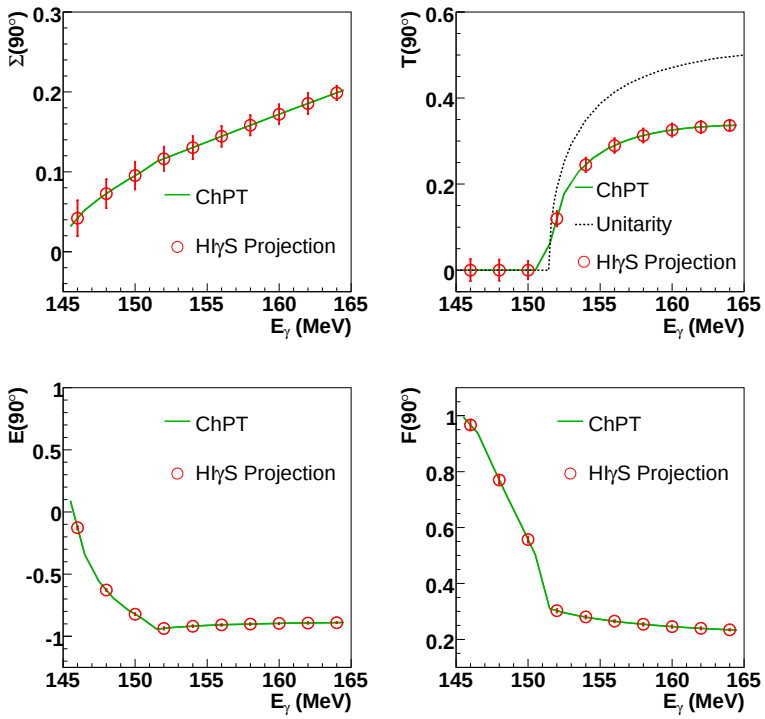

Figure 7: Predicted polarization asymmetries as a function of photon energy at a pion CM angle of 90^0 for the $\vec{\gamma}\vec{p} \to \pi^0 p$ reaction. The upper panels show the $\boldsymbol{A(y) \equiv T(90°)}$ and $A(\gamma) \equiv \Sigma(90°)$ predictions versus photon energy, while the lower panels display the predictions for $E(90°)$ and $F(90°)$ versus energy. The solid curves starting at the $\pi^+ n$ threshold correspond to the ChPT predictions [21] (see text for discussion). The dotted curve shown for the case of the $T(90°)$ (upper right) is the result of a fit based on unitarity (see text). The points show projected statistical errors at various photon energies for 100 hours of running time each at HIγS. See Table 2 for definitions.

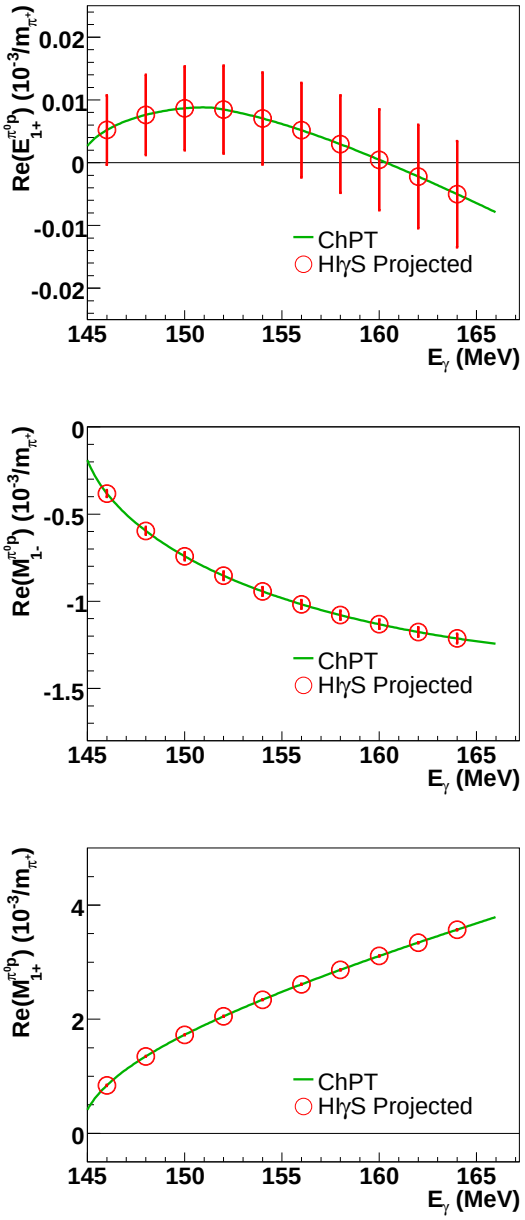

Figure 8: Top: Re (E_{1+}), Middle: Re (M_{1-}), Bottom: Re (M_{1+}) for the $\gamma p \to \pi^0 p$ reaction. The solid curves are a ChPT [18, 19, 20, 21] calculation. For all panels the projected data points show the estimated statistical errors for 100 hours of beam time at HIγS at each energy in four different beam-target polarization configurations (see Fig. 7).

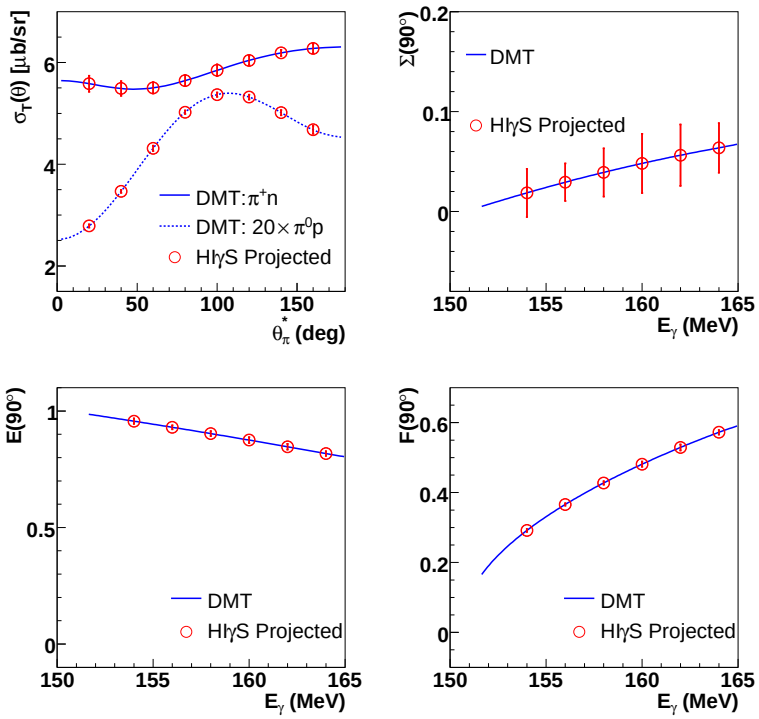

Figure 9: Predicted cross section for the $\pi^0 p$ and $\pi^+ n$ channels at a photon energy of 164 MeV (upper left). The time reversal even polarization asymmetries as a function of photon energy at a pion CM angle of 90° for the $\vec{\gamma}\vec{p} \to \pi^+ p$ reaction using the DMT model [50, 83] are shown in the other three panels. The data points show the projected statistical uncertainties for 100 hours of running at HIγS for each data point. The calculated time reversal odd asymmetries are all small in this energy range and are not shown. See Table 2 for definitions.

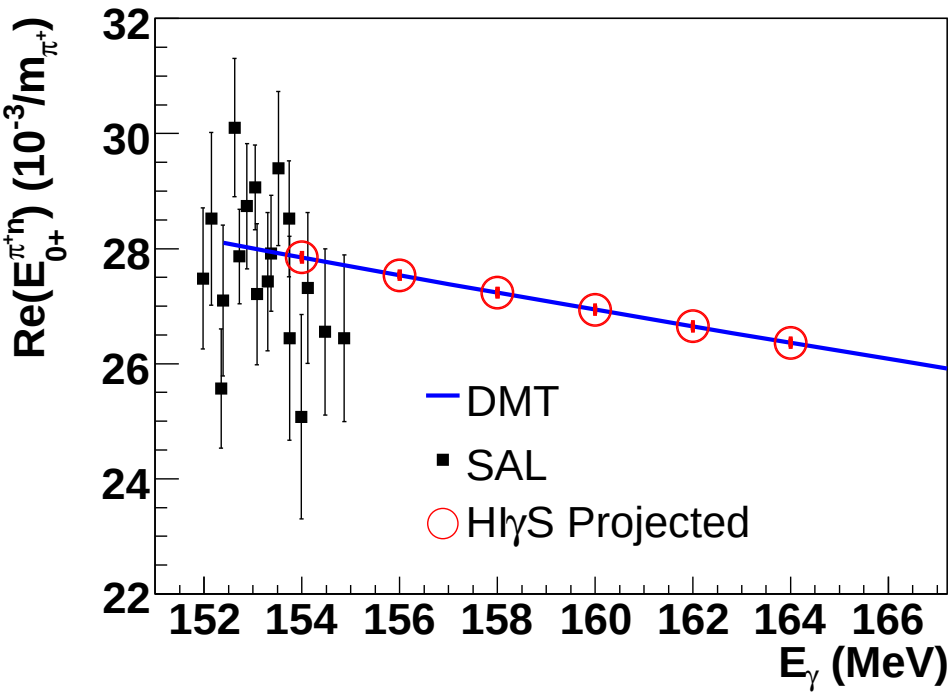

Figure 10: Re (E_{0+}) for the $\gamma p \to \pi^+ n$ reaction. The curve is DMT [50] and the square data points are from SAL [48]. The projected data points show the estimated errors for 100 hours of beam time at HIγS at each energy in four different beam-target polarization configurations (see Fig. 9).